ABSTRACT

Title of Thesis: EHD-ENHANCED HEAT TRANSFER IN A METALLIC AND A CERAMIC, COMPACT HEAT EXCHANGER

Degree candidate: Bruce Edward Baumgarten

Degree and year: Master of Science, 2003

Thesis directed by: Dr. Michael M. Ohadi

Professor

Department of Mechanical Engineering

Electrohydrodynamic (EHD) heat transfer enhancement has enormous potential to increase heat transfer rates while minimizing heat exchanger size. The aircraft industry, for one, could benefit using EHD heat transfer enhancement. Engineers can change their design approach and plan for minimal loads, resulting in heat exchangers more suitable to avionic geometries, allowing for additional payload space. During normal and operationally-induced increased heat loads, an EHD cooling system could automatically adjust the heat exchanger's capacity to handle these loads. The research goal is to prove a viable EHD heat exchanger concept while moving the technology towards commercial acceptance. Two concepts are investigated. One considers a common metallic material, while the other investigates ceramic construction. Both concepts show promise and

advance the technology. The metallic EHD-enhanced heat exchanger yielded heat transfer rates nearly three fold compared to conventional heat exchangers, thus introducing a potential for three times reduction in the heat exchanger size.

EHD-ENHANCED HEAT TRANSFER IN A METALLIC AND A CERAMIC COMPACT HEAT EXCHANGER

by

Bruce Edward Baumgarten

Thesis submitted to the Faculty of the Graduate School of the
University of Maryland, College Park in partial fulfillment
of the requirements for the degree of
Master of Science
Fall 2003

Advisory Committee:

Professor Dr. Michael M. Ohadi, Chair
Professor Dr. Reinhard Radermacher
Associate Professor Dr. Tien-Mo Shih

DEDICATION

I wish to thank my wife, Catherine,
and my children, Sarah, Rachel, Emily, Nora, Meg, and Jack
for their patience and continuing support throughout my educational career.

ACKNOWLEDGEMENTS

I would like to express my thanks to all personnel from the Enhanced Heat Transfer Laboratory at the University of Maryland. Drs. Dessiatoun, Molki, and Ivankhenko have greatly contributed to the outcome of the project, and have provided extremely beneficial technical and educational knowledge and experience. In addition, I would like to especially thank Tony McNair, Drs. Mohsen Salehi, Jafar Darabi, and Ashok Gidwani, all my fellow students then, for their support - technical, educational, and moral.

TABLE OF CONTENTS

NOMENCLATURE

β	Area Density
$\dot{q}$	Heat Transfer Rate
U	Overall Heat Transfer Coefficient
A	Heat Transfer Surface Area
ΔT	Temperature Difference
V	Fluid Flow Volume
$\overline{f_e}$	Electric Body Force
ρ_c	Electric Field Space Charge Density
E	Applied Electric Field Strength
ε	Dielectric Permittivity
ρ	Mass Density
ε_{hx}	Heat Exchanger Effectiveness
C_p	Specific Heat
w	Measured Weight
$\sigma_{max\ theor}$	Maximum Theoretical Strength
E	Elastic Modulus
σ	Applied Stress
ε	Strain
$\dot{q}''$	Rate of Heat Transfer per unit area
k	Thermal Conductivity
α	Coefficient of Thermal Expansion
$\sigma_{thermal}$	Thermal Stress
μ	Poisson's Ratio
ΔT_c	Critical Temperature Difference
k_{Ic}	Fracture Toughness
c_i	Average Flaw Size
σ_i	Standard Deviation of variable i
u_Y	Uncertainty in variable Y
h	Enthalpy
X	Refrigerant Quality

LIST OF FIGURES

LIST OF TABLES

LIST OF ABBREVIATIONS

EHD	Electrohydrodynamic
LMTD	Logarithmic Mean Temperature Difference
CFC	Chlorofluorocarbons
HCFC	Hydrochlorofluorocarbons
HFC	Hydrofluorocarbons
PAO	Polyalphaolefin
kV	kilo Volt
NMES	Nonmetallic Elemental Solid
APF	Atomic Packing Factor
FCC	Face Centered Cubic
HCP	Hexagonal Close-Packed
BCC	Body Centered Cubic
psi	Pounds per square inch pressure
FRC	Fiber Reinforced Ceramics
HB	Brinell Hardness
HR	Rockwell Hardness
HV	Vickers Hardness
HK	Knoop Hardness
SBR	Styrene Butadiene Rubber
Re	Reynolds Number

Chapter 1

INTRODUCTION

Compact heat exchangers have been studied in great detail, and their heat transfer characteristics have been proven over many years. More recently, electrohydrodynamic (EHD) heat transfer enhancement, an active enhancement method, has produced dramatic improvements in the heat transfer coefficients of many heat exchanger fluids. Experiments have shown promising results, but development of practical heat exchangers is still needed. This study introduces the EHD enhancement technique into a metallic, five-port, compact heat exchanger and proves the feasibility of miniaturization in a simple tube-in-tube heat exchanger. Additionally, the introduction of ceramics in the construction of the heat exchanger shows potential advantages previously considered unattainable for practical applications.

The EHD technology, due to its potential in increasing heat loads and minimizing size requirements, has enormous potential application in the aircraft industry, where the age-old doctrine of "higher, faster, farther" has been the guiding principle of each design iteration over the decades. This doctrine is not without its limits, however, and it would be appropriate to add "affordable and smart" to the list of principles. The main challenge for the aircraft industry in the 21st century is to provide technologically superior products and services at an affordable price. Implementation of EHD into aircraft design can help meet this challenge and design approach. The development of such technologically superior heat exchangers at a reduced size and weight would be a phenomenal achievement. Engineers could design heat exchangers for minimal or average heating or cooling loads such that any needed increase in heat transfer could be

handled by a simple, controllable applied electric field or EHD potential (voltage) adjustment. How much "smarter" could a design be? Typically, the voltages required to enhance the heat transfer associated with EHD are accompanied by very low current values, resulting in power consumptions that are very small, and are much smaller than traditional technologies on the same enhancement basis. The most significant drawback when discussing most enhancement techniques, pressure drop, can also be significantly reduced using EHD when compared to other techniques, both active and passive. This controllable feature of EHD heat exchangers can provide highly stable temperatures so that the reliability of any electronic equipment, cooled by the fluid passing through the heat exchanger, is improved.

Most aircraft subsystem heat exchangers are considered compact, with small internal passages and large heat transfer areas. The small passages in compact heat exchangers are well suited for EHD enhancement, since in small channels the flow is predominantly laminar and EHD enhancement is most pronounced in a laminar regime. The EHD-induced secondary motions are more effective in laminar flow than they are in a well-mixed turbulent flow regime. The EHD-induced secondary motions disturb the thermal boundary layer near the heat transfer surface; allowing more effective momentum exchange, thus a lower resistance in the boundary layer and higher resulting heat transfer coefficients. The development of efficient EHD heat exchangers not only has potential application in the aircraft industry, but also in other conventional industries such as power and process industries, where additional energy efficiency can lead to reduced costs and environmental emissions.

Developmental issues, from analytical development to product manufacturing and producibility, still remain problematic for researchers. Many hurdles need to be overcome for EHD to be a viable product in actual use; most of these hurdles deal with manufacturing and implementation of electrode configurations into the body of the heat exchanger. Experiments have been conducted by previous researchers on a small scale, such as a wire electrode inside a tube, but unfortunately, although previous results have been very promising, the transfer of the technology to more rugged designs with multiple passages has been slow to develop.

The basic and application-oriented work completed for this study will, therefore, be an extremely beneficial tool for the development of technology transfer to actual usage in environments and applications where EHD can have an enormous impact. The results for the five-port HX show very promising trends, and the data collected shows significant miniaturization possibilities. The results for the ceramic HX also show encouraging trends, but unfortunately, no extensive data has been acquired to substantiate the enhancement levels attainable with the EHD technique in a ceramic, compact heat exchanger. However, the difficulties encountered with the ceramic HX have considerably advanced the technological know-how in further development of EHD-enhanced ceramic heat exchangers.

Chapter 2

EHD ENHANCED HEAT TRANSFER FUNDAMENTALS

2.1 Introduction

This chapter provides an introduction to various categories of heat exchanges first, and will be followed by a review of the fundamental aspects of the electrohydrodynamic enhancement of heat and mass transfer. In the last section of this chapter, a review of previous related work is presented.

2.2 Size Classification

Compact heat exchangers are classified as such based on the area density, β, of the heat transfer surface. Area density is defined as the ratio between the heat transfer surface area and the corresponding flow volume of the fluid. The typical area density cutoff for a heat exchanger to be considered compact is approximately 700 m^2/m^3 (213 ft^2/ft^3) (London, 1980). This cutoff value translates to a tube with an equivalent circular, or hydraulic, diameter of 5.7 mm (.224 in.). Therefore, a heat exchanger employing channels with a hydraulic diameter of 5.7 mm (0.224 in.) or less would be considered compact. For comparative purposes, the human lung has a β of almost 20,000 m^2/m^3 (6086 ft^2 / ft^3), with an equivalent hydraulic diameter of 0.1 mm or 100 microns (0.004 in.). Higher β geometries result in heat exchanger channels with smaller equivalent hydraulic diameters. A heat exchanger with area density in the range of 2500 m^2/m^3 (761 ft^2/ft^3) up to 10,000 m^2/m^3 (3,043 ft^2/ft^3) is considered sub-compact. A heat exchanger with area density greater than that of the sub-compact range is considered a micro-

channel heat exchanger, or over 10,000 m^2/m^3 (3,043 ft^2/ft^3). The present research deals with a sub-compact heat exchanger, with a β greater than 2500 m^2/m^3 (761 ft^2/ft^3) and less than 10,000 m^2/m^3 (3,043 ft^2/ft^3).

2.2.1 Heat transfer theory

A compact heat exchanger by name is not necessarily of small total unit volume and mass; rather, the area density β, wherein heat transfer occurs, is high. The high area density allows significantly higher heat removal rates to be attained, due to the additional surface area utilized. The following derivation (London, 1980) illustrates the usefulness of compact heat exchangers. The fundamental equation for rate of heat transfer is**:**

$$\dot{q} = U\ A\ \Delta T \tag{2.1}$$

where q is the heat transfer rate, U is the overall heat transfer coefficient related to the heat transfer area, A is the heat transfer surface area, and ΔT is the temperature difference. The temperature difference is sometimes replaced with the logarithmic mean temperature difference (LMTD), especially in counter-flow heat exchangers, where the two fluids are passing each other in opposite directions. Consider the heat transfer area in terms of β:

$$\beta = \frac{A}{V} \tag{2.2}$$

where A is the heat transfer surface area and V is the fluid flow volume of the heat exchanger channel. Therefore, following substitution, the heat transfer rate (2.1) can be rewritten as:

$$\dot{q} = U V \beta \Delta T \qquad 2.3$$

Clearly, from this simple derivation, it is obvious that smaller volume heat exchangers can be realized with higher β geometries while keeping the overall heat transfer coefficient constant. A greater heat transfer rate can also be achieved with a heat exchanger occupying the same space and volume.

2.3 High Performance Characteristics

The EHD enhancement technique of heat transfer is an active form of heat transfer augmentation that utilizes the effect of electrically induced secondary motions that are produced when a high voltage, low current electric field is applied to a dielectric fluid medium. These secondary motions improve mixing in the bulk flow and increase the activity near the heat transfer surface, leading to heat transfer coefficients that are often an order of magnitude higher than those achieved by conventional enhancement techniques. The magnitude and nature of the enhancement is a direct function of electric field and flow field parameters, as well as heat transfer surface conditions.

The force behind the electrically induced secondary motions is the electric body force (Landau and Lifshitz, 1960, Stratton, 1941, and Woodson and Melcher, 1985). An electric field, when applied across a fluid medium with low electrical conductivity, creates the necessary interactions between the electric, temperature, and fluid flow fields

to produce secondary motions. The mathematical representation of this force (Landau & Lifshitz.), on a volumetric basis, is:

$$\overline{f_e} = \rho_c E - \frac{1}{2} E^2 \nabla \varepsilon + \frac{1}{2}\left[E^2 \rho \left(\frac{\partial \varepsilon}{\partial \rho} \right)_T \right] \qquad 2.4$$

where ρ_c is the electric field space charge density, E is the applied electric field strength, ε is the dielectric permittivity of the fluid, ρ is the mass density, and T is the temperature. The electric body force can be split into three distinctive forces: the Coulomb force, the dielectrophoretic force, and the electrostrictive force (Figure 2.1). The force associated with free charges in the medium is the Coulomb force, the first term on the right hand side of the equation. In a single-phase flow, the Coulomb force is the dominant contributor to the EHD body force and the resulting heat transfer enhancements. The second term on the right hand side of the equation is the dielectrophoretic force, which arises from the spatial change of dielectric permittivity within the fluid medium. Boiling/evaporation, condensation, melting, and freezing are practical examples where a strong $\Delta\varepsilon$ contribution to the electric body force leads to substantial enhancements in the heat transfer coefficient. The third term in the body force equation, referred to as the electrostrictive force, is associated with the inhomogeneities in the applied electric field, the density gradients, and the resulting changes in ε. Therefore, the electrostrictive force contributes to the EHD body force in two-phase flow processes, due to the dielectric gradient at the phase separation line, and in situations

where a non-uniform electrical field, often encountered in enhanced heat transfer surfaces or unusual electrode configurations, is present in the fluid medium.

The three types of EHD interactions- gas, liquid, and two-phase - incorporate the EHD body force in heat transfer enhancement. Gas phase (air) convective heat transfer interactions normally involve ionization of the gas or the discharge of corona, which occurs when charged particles (ions) in the gas migrate to the electrode with the opposite charge. This corona discharge causes additional flow in the fluid medium. The simple presence of a charged electrode in air disturbs the air around the electrode and increases heat transfer. Many interactions that involve the liquid phase deal with polarization of the fluid particles. Dielectric liquids, such as most refrigerants (CFCs, HCFCs including R-134a, & HFCs) and oils (PAO), polarize when influenced by an electric field (Figure 2.2). In figure 2.2a, with no EHD effects, electrical dipoles do not assume any particular configuration, whereas under the influence of EHD, the dipoles align themselves according to the electrode configuration (Figure 2.2b, c.) The net movement of fluid particles is in the directions of the region of greatest electric field intensity. For additional information on EHD principles, applicability, and limitations, see Ohadi et al., 1991, Yabe, 1991, Singh et al., 1993, and Ohadi et al., 1994.

2.3.1 Heat Exchanger Effectiveness

A common yardstick for heat exchanger comparison is the concept of effectiveness. The effectiveness of a heat exchanger is defined as the ratio of actual heat transferred to maximum possible heat transfer:

$$\varepsilon_{hx} = \frac{q}{q_{\max}} \qquad 2.5$$

$$\varepsilon_{hx} = \frac{C_{p\text{-}hot}\left(T_{hot\text{-}i} - T_{hot\text{-}o}\right)}{C_{p\text{-}hot}\left(T_{hot\text{-}i} - T_{cold\text{-}i}\right)} \qquad 2.6$$

where ε_{hx} is the effectiveness, C_p is the specific heat of the fluid, the subscripts *i* and *o* are inlet and outlet locations, respectively. The numerator of equation 2.6 can be the heat transferred for either the hot or cold fluid due to conservation of energy across the heat transfer surface.

2.4 Previous Work

A study by Tran, Wambsganss, France, and Jendrzejczyk (1993) on the boiling heat transfer in small, rectangular channels concluded that heat transfer is enhanced when using compact geometries. Their explanation for the enhancement was based on surface tension effects, which thinned the liquid film on the heat exchanger walls, creating a disturbed flow to transport the heat. They determined that the state-of-the-art correlations for in-tube evaporation significantly under-predicted heat transfer rates for compact geometries.

H.Y. Choi (1968) investigated the effects of strong electric fields on condensation heat transfer. Choi condensed R-113 inside a vertical tube and conducted experiments with and without an applied electric field. His results showed that, at a maximum applied voltage of 30 kV, heat transfer increased from 50 - 100 %, depending on the mass flow of the inlet vapor. Decreasing mass flow increased the enhancement achieved. High

electric field heat transfer data correlated well when compared to a model using modified Nusselt and Rayleigh numbers. Choi determined that the EHD force and wavelength are important parameters in the correlation and concluded that the subsequent correlations were successful only for the high electric field data.

Yabe, et al. (1991) studied the effect of the EHD phenomenon on condensation heat transfer for development of a high-performance heat pump. The condenser was a shell and tube type with R-114 as the working fluid. With an applied voltage of 21 kV, an enhancement of approximately 600% was achieved under constant heat flux. Yabe et al. concluded that: (a) the electric power consumption of the electrodes used to achieve the enhancement, compared to the amount of heat exchanged, was negligible (on the order of 0.001 %); (b) the EHD technique is effective for films with Reynolds numbers larger than 1000; and (c) the deleterious effect of lubricating oil on the heat transfer was negligible (less than 0.1 %), although the power consumption was approximately 20 – 30 times greater than iterations without oil.

Holmes and Chapman (1970) condensed R-114 in the presence of a non-uniform, alternating electric field. The experiment created the non-uniform field by adjusting the angle between two plates, one as the condensation surface and the other as a plate electrode. Results showed that for parallel plates, no enhancement was experienced due to the alternating current. Once an angle was introduced between the plates (as little as 6°), non-uniformities were produced in the electric field strength, which provided enhancement values up to and over 1000%.

A common problem with the engineering of ceramic heat exchangers is designing the heat exchanger so that structural stability is maintained. In 1985, C. Bliem, et al.,

researched several designs of ceramic heat exchangers in industrial applications. All of the designs experienced problems with seal leakage. A distinct problem with ceramics is the disinclination of ceramic parts to bond with other ceramic and metallic materials. Since Bliem's research, and before, the main area of research has been in solving this problem without incurring detrimental effects to the desired properties.

Custer and Simpson in 1995 received a patent for their unique solution to this structural integrity problem. Their approach changed the heat exchanger design rather than the sealing mechanism. They incorporated a hollow ceramic outer tube secured to a corrugated inner ceramic tube into the design. The openings between the two tubes and the inner annulus constituted the many fluid passages. The design is premised on the fact that the ceramic would fail and that the researchers would be unable to prevent the failure. The purpose of the corrugated inner member is to prevent the catastrophic failure of the outer tube by momentarily slowing the momentum from the failed outer member. This design was incorporated in a multi-tube heat exchanger to prevent the shrapnel-like action of a failed tube from damaging surrounding tubes.

In 1996, Lashbrook et al. received a patent for their solution to the sealing problem. They incorporated an annular seal around the ceramic tube inserted in the base of the heat exchanger. Since the tube was not connected to the plate, as the temperature increased, the ceramic could expand. The expansion increased the diameter of the tube and created a tighter seal on the O-ring. This simple solution did not account for additional stresses placed on the material, which would still cause catastrophic failure due to the brittleness of the ceramic. The only difficulty was to choose a sealing material that would not degrade under the particular environment suitable for ceramics.

For plate heat exchangers, Linsner et al. designed a process that sealed the plates together using differential pressures and a liquid synthetic resin. During the fabrication of the plate heat exchanger, the eventual cold side passages were filled with the resin either under high pressure and allowed to cure, or under atmospheric pressure while placing the eventual hot side passages under a vacuum. This particular process is especially suitable for heat exchangers made of silicon nitride or silicon carbide. With these materials, it is advantageous to mechanically clean the passages before the resin treatment. A high viscosity abrasive was pumped through the passages to remove the silicon nitride or silicon carbide whiskers that are a result of the reaction firing fabrication process.

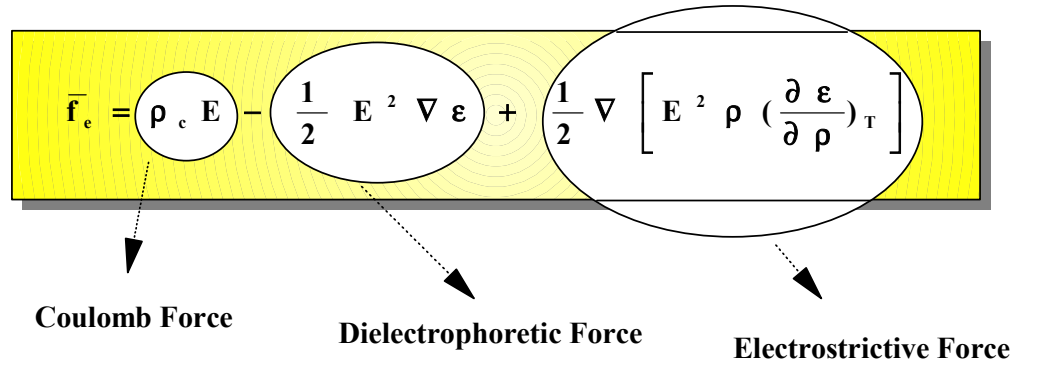

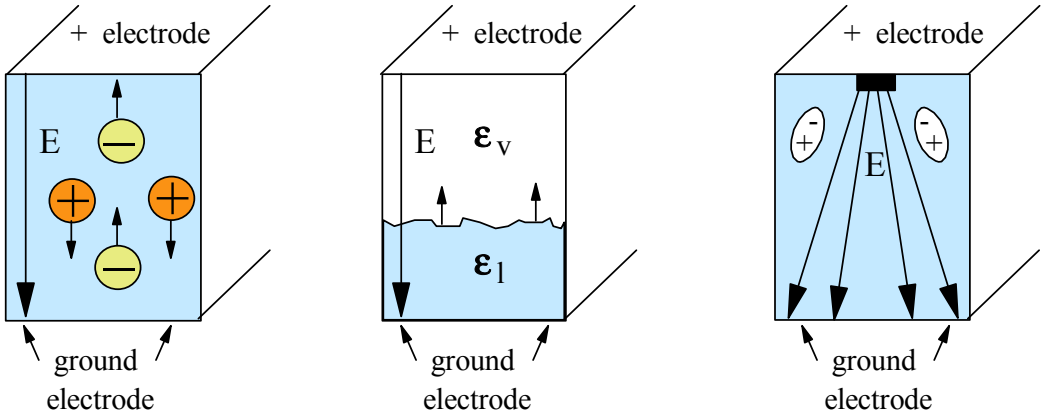

Free Ions / Charges

Significant in Single Phase (liquid)

The coulomb force always exists

$\varepsilon_l >> \varepsilon_v$

$\nabla\varepsilon$ is significant in phase change processes due to high permitivity gradient at the liquid-vapor interface

∇E^2 is significant when there is a non-uniform electric field intensity created by an irregular surface or electrode geometry

can be combined by having a two-phase mixture in the presence of a non-uniform electric field

Figure 2.1 : EHD Body Force Equation

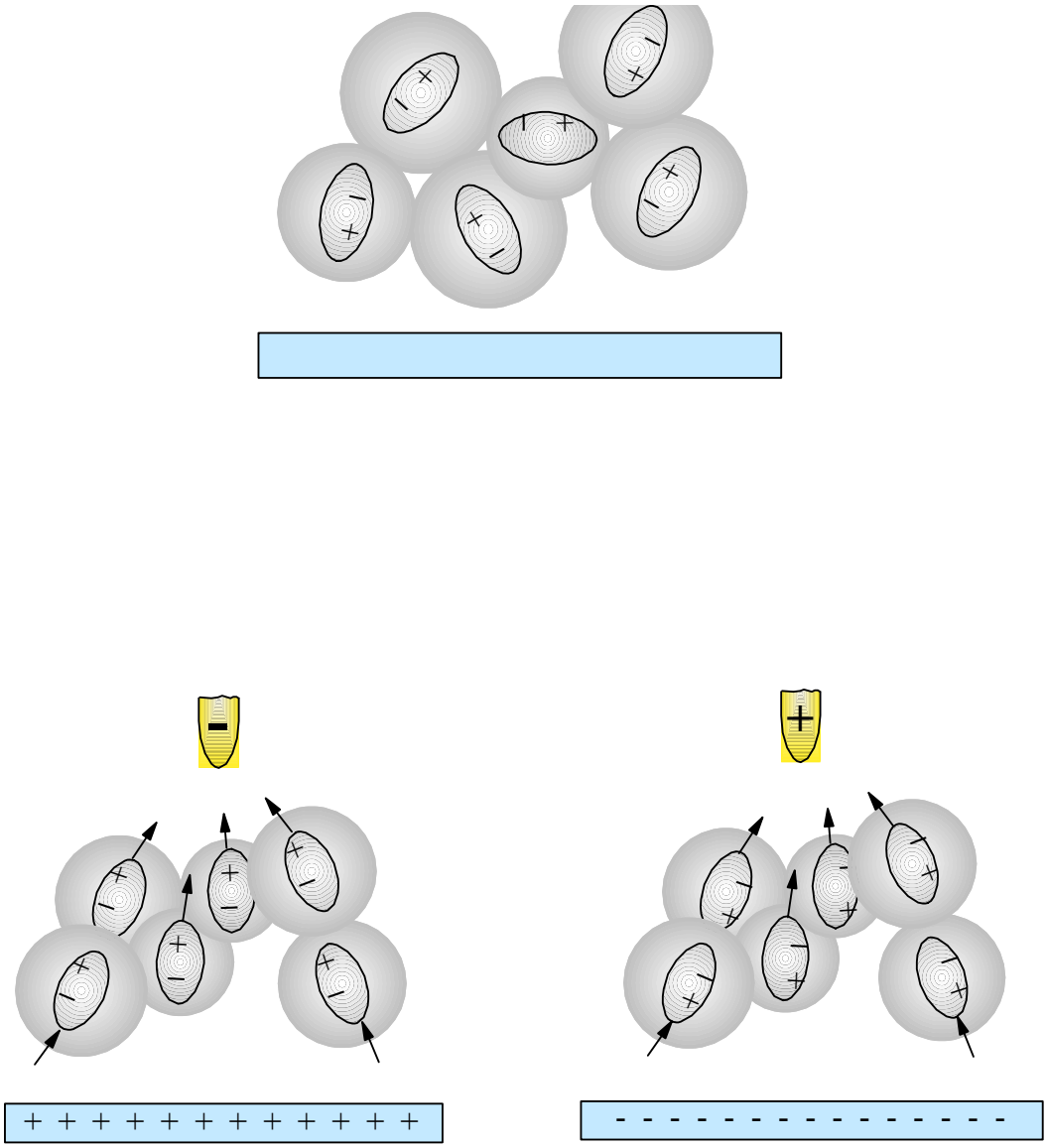

Figure 2.2 : EHD Polarization of a Dielectric Fluid

Chapter 3

ALTERNATIVE HEAT EXCHANGER MATERIALS

3.1 Introduction

Most heat exchangers in use today are constructed of metallic materials. Ceramics are not used as frequently due to their inherent insulating properties. However, metals have their own drawbacks when used for an EHD heat exchanger. Metals serve as excellent conductors of both heat and electricity, but the metallic heat exchangers will not benefit from the electrical conduction necessary for EHD unless the heat exchanger is sufficiently insulated to allow a voltage to build up across the fluid medium. This insulation process is significantly easier to implement when compared to insertion of the EHD technology into a ceramic heat exchanger. There are only a handful of ceramic materials that actually have decent heat transport properties, and even fewer that display other desired properties needed for the EHD technique to be successful. Although there are few, those ceramic materials that have the potential for use in EHD heat exchangers are worth investigating due to the potential that the material possesses.

3.2 Ceramic Heat Exchangers

The high cost of energy has led industry to find methods of extracting usable heat from high temperature waste streams. The use of ceramics in the design of heat exchangers is relatively new, developing in the last 20 to 25 years. Certain unique ceramic properties allow formerly impossible applications to be achieved. Ceramics can be used in and designed for heat exchange applications because of their ability to retain many of their properties at elevated temperatures of above 800 °C. Such applications

might include the recovery of heat energy from industrial waste heat processes. Another ideal property of ceramics is their hardness. This property lends itself to use in heat exchange processes where corrosive liquid and/or gases are used. Ceramic materials are ideal for use in heat exchangers in specific processes and applications (Heinrich, 1990). Chemical applications include the elevation of acid concentrations and heat recovery of concentrated hot acids. Industrial applications include preheat treatment of combustion air by the flue gases of industrial furnaces. Thermal cleaning systems' corrosive flue gases can be preheated and the exhaust gases can be cooled down below the dew point of the cleaning acid.

A very common problem with the engineering of ceramic heat exchangers is designing the heat exchanger so that structural stability is maintained. In 1985, Bliem et al. researched several designs of ceramic heat exchangers in industrial applications, and all of the designs experienced problems with seal leakage. A problem with using ceramics is their inability to bond with other ceramic and metallic materials. Even before Bliem's research, the main research focus has been in solving the problem of bonding ceramics to other parts of the system without incurring detrimental effects on the desired properties. Past researchers, such as Custer and Simpson (1995), Lashbrook (1996), and Linsner (1989) developed strategies to overcome certain drawbacks, as stated in chapter 2, and have given current and future engineers hope in resolving issues that create hesitancy for use of ceramics in heat exchange applications.

The research presented here investigates many ceramic properties to better understand past failures and use the information to design a ceramic heat exchanger

capable of EHD heat transfer enhancement. Those properties discussed play a major role in heat transport capability, constructability, or operating integrity.

3.3 Material Background

There are three main categories involved with the science of materials: metals, non-metals (or gases) and nonmetallic elemental solids (NMESs). Very few solids are used in their natural, pure form; rather solids are engineered for performance based on their intended use. Engineered solids include engineered metals, polymers, and ceramics, or semi-conductors. The mechanical properties of solids depend largely on the type of bonding which holds the molecules together. Metals use metallic, or ionic, bonding, where valence electrons are given up to fill another molecule's electron shell. Polymers use covalent bonding, wherein the valence electrons are shared between molecules, which bond the molecules together and provides a type of secondary bonding that holds the carbon chains together. These secondary bonds (Van der Waal or Hydrogen) dictate the properties of polymers. Secondary bonding is of significant importance, as a material is only as strong as its weakest link. Ceramics use both ionic and covalent bonding to hold the molecules together. According to Barsoum (1997), ceramics are defined as

> *Solid compounds that are formed by the application of heat, and sometimes heat and pressure, comprising at least one metal and a nonmetallic elemental solid (NMES), a combination of at least two nonmetallic elemental solids, or a combination of at least two nonmetallic elemental solids and a nonmetal.*

In addition to the type of bonding, the mechanical properties of solids, especially ceramics, depend largely on the arrangement of the atoms in the molecule. A unit cell is the smallest repeatable region in a material that describes this arrangement. Seven types of unit cells, characterized by six parameters, describe the basic geometry. These

parameters are known as lattice parameters and describe the edge lengths of the unit cell and the angles between these edges in three-dimensional space. The majority of ceramic materials are crystalline compounds. The molecules of crystalline compounds exhibit long-range order, which is best described as an arrangement of atoms whose repeatable pattern is much greater than the individual bond lengths between the atoms. The other type of order a solid can exhibit is short-range order, in which the atoms in a solid exhibit periodicity only in lengths approximate to the dimensions of the molecule's bond lengths. This type of atom arrangement characterizes solids known as amorphous, glassy, or non-crystalline solids.

Since most ceramics exhibit long-range order, this discussion will mainly concern crystalline compounds. Crystalline solids can be composed of either single crystals or numerous groupings of single crystals and polycrystalline solids. Single crystals exhibit the perfect, repeated arrangement of atoms throughout the entire compound, while polycrystalline solids have crystals grouped in clusters called grains. Individual grains still possess long-range order, but each group, or grain, may be oriented in a different direction from neighboring grains. This region of separation is called a grain boundary and is characterized by disorder where the two orientations meet. A compound's micro-structure consists of the shape and size of its grains, in addition to other factors, including porosity and secondary phases. Many ceramic properties are dependent upon the micro-structure of the material.

Ceramics are not a new invention. The use of ceramics is as old as civilization itself. In most archeological digs, pottery and sculptures are commonly the majority of the artifacts excavated from previous civilizations. These ceramics are known as

traditional ceramics and are quite abundant since the materials used in their production make up approximately 95% of the earth's crust. Silicon dioxide and silicates make up the outermost solid layer of the planet in the form of rocks and soil. Structural clay products are classified as traditional ceramics and are comprised of silicates with a coarse, non-homogeneous, multi-phase micro-structure.

Advanced ceramics, on the other hand, are a fairly recent invention. These ceramics are not clay- or silicate- based, but use raw materials like oxides, carbides, and completely synthetic materials. The advantage of these engineered ceramics is that their micro-structures are usually much finer (by an order of magnitude), less porous, and more homogeneous compared to the traditional ceramics. These micro-structure parameters make engineered ceramics better suited for use in today's technical society, potentially for use in heat transfer applications due to their micro structure homogeneity, allowing for more controlled heat transport.

3.4 Ceramic Properties of Interest to Heat Exchanger Design

As with all engineered materials, ceramics have both detrimental and beneficial properties, which can be manipulated through the use of composites to degrade unwanted properties, or enhance desired properties. In pure ceramic compounds, certain properties are unique to ceramics simply because of their structure. The properties discussed below have been selected due to their direct or indirect relation to the thermal interests of heat exchanger design.

Atomic Packing Factor: Many properties exhibited by ceramic compounds are determined by their crystal structure. The arrangement of the unit cell and the location of

the compound's cations and anions (positive and negative ions) dictate the crystal structure. According to Colling (1995), a useful parameter for understanding ceramics is the atomic packing factor (APF). This parameter is the volume fraction of atoms occupying the unit cell and can be determined from the atomic radius, the geometry of the unit cell, or the density of the material; the general expression is:

$$APF = \frac{(No.\ of\ atoms\ per\ unit\ cell)(vol.\ of\ each\ atom)}{Vol.\ of\ unit\ cell} \qquad 3.1$$

The most efficient packing possible is found in face centered cubic (FCC) and hexagonal close-packed (HCP) unit cells. The APF for these arrangements is 0.74, while an APF of 0.68 is found in body-centered cubic (BCC) structures. These factors are the maximum possible for the particular arrangement, based on a pure substance of one element. Since ceramics incorporate more than one element, and atoms of the unit cell have different radii and may not touch one another, ceramic's APF values are much lower, as low as 0.35. These low APFs are crucial to attaining favorable ceramic properties for heat exchangers, especially from a minimum thermal expansion point of view.

Density: Another property related to APF is density. The greater the atomic mass, the denser the solid will be. Ceramic densities have a wide variety of values, but for current widespread technological use, low-density ceramics are desired. Lower densities correspond to reduced component weight. Ceramics that incorporate covalent bonds are more 'open' structures leading to a lower density than those materials that use ionic bonding. Density in ceramics can change depending on the ceramic and the applied manufacturing procedures (discussed in more detail later). Many ceramics are formed under pressure and/or temperature differences that can greatly affect the density. Because

the manufacturing methods and parameters vary, the actual density may not achieve the theoretical density. The fractional density describes the ratio between actual and theoretical densities:

$$\rho_{frac} = \frac{\rho_{actual}}{\rho_{theoretical}} \qquad 3.2$$

A greater fractional density, ρ_{frac}, improves the density distribution, which controls the homogeneity of other mechanical properties. Theoretical values can be found listed in many references, but the general formula is as follows:

$$\rho_{theoretical} = \frac{(atoms / cell)(atomic\ mass / atom)}{(unit\ cell\ volume)(Avogadro\ no.)} \qquad 3.3$$

where the Avogadro number is 6.02×10^{23}. An accurate method to determine the actual density is to use the Archimedes principle:

$$\rho_{actual} = \frac{w_{air}}{(w_{air} - w_{fluid}) / \rho_{fluid}} \qquad 3.4$$

where w is the measured weight in the corresponding medium and ρ is the density. The measurement of the actual density can prove to be difficult due to the porosity of some ceramics.

Mechanical Strength: According to Barsoum (1997), most atomic bonds break when the inter-atomic distance is stretched by approximately 25%. Barsoum also proved by a simple geometric construction that the theoretical strength of a solid is roughly one-tenth of its elastic modulus value:

$$\sigma_{maximum\ \ theor} = \frac{E}{10} = \frac{\sigma}{10\,\varepsilon} \quad \Big| \, at\ r \approx r_0 \qquad 3.5$$

where E is the elastic modulus, and σ and ε are the applied stress and corresponding strain at an inter-atomic distance r close to the equilibrium distance of r_o. Ceramics, however, defy this theoretical construction: their maximum allowable stress is only 1/1000 to 1/100 of the value of the corresponding elastic modulus. The reason for this altered relationship is that ceramics, like all solids, are not perfect in micro-structure. All solids contain flaws and defects that locally concentrate the applied stress in the area of the defect, which is unforgiving in the brittle ceramic micro-structure. Ceramics are brittle by nature due to the ionic bonding, and their tensile strengths can vary over a wide range of values (several hundred to over a million psi.) Single crystal whiskers, fine fibers with a large length-diameter ratio, occupy the high end of the ultimate tensile strength values, while ceramics in bulk form rarely have tensile strengths above 25,000 psi. This value is relatively low compared to other materials, especially metals. Because ceramics are brittle, they do not plastically deform like metals, and cannot handle any additional energy, whereas metals can handle a tremendous amount of additional energy before failure. Again, this drastic difference in material behavior comes from the bonding at the atomic level. Ceramics also demonstrate a difference in their compressive strengths, typically about five to ten times greater than their tensile strengths. In most instances, employing ceramics in composite materials or as fiber-reinforced ceramics (FRC) drastically improves the strength properties and can be beneficial to the type of application needed.

As mentioned previously, the grain size of a ceramic material can greatly affect

the properties of the final product. Advanced ceramic grains are much smaller than those of traditional ceramics, and usually are much stronger. In fact, the strength of the ceramic product is inversely proportional to grain size and directly related to size homogeneity. Since advanced ceramics possess smaller grains and more homogeneity, they are much more useful than traditional ceramics in terms of strength.

Thermal Conductivity: Thermal conductivity is the property that reflects the rate of heat flow per unit thickness through a material. Heat is conducted through solids due to thermal gradients. Analogous to Fick's law, a relationship exists between thermal gradients and heat flux applied to the material:

$$q'' = -k \Delta T \qquad 3.6$$

where k is the thermal conductivity of the material, q" is the total rate of heat transfer per unit area, and ΔT is the temperature gradient. The heat flow is governed by the amount of energy present that is transported through the transfer of free electrons or, in ceramics, via lattice vibrations, commonly known as phonons. Some references confuse the phonon theory by defining them as particles. These phonons are nothing but an abstract vibratory motion of the lattice parameters between unit cells. Phonons transport heat much more efficiently when the crystal structure is least cluttered. As with other properties, ceramics exhibit a wide range of thermal conductivities. The ceramics with high thermal conductivities are those that have the least cluttered structures. The least cluttered structures are those made of single elements, elements of similar atomic weight, and/or no extraneous atoms. An example of a single element structure is diamond, with a

thermal conductivity more than five times that of copper. Beryllium Oxide (BeO), Aluminum Nitride (AlN), Silicon Carbide (SiC), cubic Boron Nitride (c-BN), and Boron Carbide (B_4C) are examples of compounds with elements having similar atomic weights and high thermal conductivities. Thermal conductivity drastically decreases as the atomic weight of the cation is increased, proof that the difference in atomic weight plays a major role in this property. In addition to differing cation weights, the introduction of a second component in solid solution will also decrease the material's conductivity. The manufacturing process also plays a big role in the conductivity of ceramics. For instance, hot pressed Silicon Carbide has a thermal conductivity of 90 W / m-K while reaction bonded Silicon Carbide can have a thermal conductivity of over 200 W / m-K. Other high values include:

Aluminum Nitride	180 - 200 W / m-K
Cubic Boron Nitride	200 - 900 W / m-K
Beryllium Oxide	260 - 300 W / m-K
Boron Carbide	90 - 100 W / m-K

Although porosity is not directly found in the equations for thermal conductivity, it can have a pronounced effect on thermal conductivity. The thermal conductivity of air is negligible when compared to that of solids, thus a large volume fraction of pores in a solid can greatly reduce the material's overall thermal conductivity value. Firebrick is a very good example of ceramics employing the use of porosity to reduce the thermal conductivity to produce a fire insulator.

Thermal Shock Behavior: Ceramics are extremely susceptible to failure due to thermal shock. Although ceramics have excellent high temperature properties, failure can easily occur during the heating and cooling of a ceramic material. These conditions cause

large temperature gradients within a substance and create a thermal stress far above the ultimate mechanical strength due to constrained material expansion or contraction. Thermal expansion is described using a coefficient of thermal expansion, α, defined as the fractional change in length with a corresponding change in temperature during a constant pressure process:

$$\alpha = \frac{l}{l_0}\left(\frac{\partial l}{\partial T}\right)_P \qquad 3.7$$

where l_0 is the original length. Compounds with low APF values tend to have low thermal expansion coefficients because any expansion is absorbed in the open spaces of the unit cell, thus minimizing expansion. Materials with APF values greater than 0.65 are close packed ionic or atomic structures: any expansion is accumulated throughout the entire structure.

Ceramics can display a wide range of thermal expansion values and typically can withstand much higher temperatures while achieving identical percentages of expansion when compared to other non-ceramic materials. Quartz (SiO_2) actually has a zero thermal expansion percentage at temperatures up to 1600 °C (2912 °F.) The mechanical stress associated with thermal gradients is:

$$\sigma_{thermal} = \frac{E\,\alpha\,\Delta T}{1 - \mu} \qquad 3.8$$

where $\sigma_{thermal}$ is the resulting stress, E is the elastic modulus, α is the coefficient of thermal expansion, ΔT is the temperature difference in the material, and μ is Poisson's

ratio. Thermal shock is a serious problem in ceramics because ceramics do not possess a stress relief mechanism like that in metals (plastic deformation). Metals undergo plastic deformation, allowing metals to absorb a much greater amount of energy than ceramics in similar situations. Under heating conditions, the outer surface of a ceramic will be in compression because of a faster expansion rate. Under cooling conditions, the faster rate of contraction of the outer surface (compared to the material's core) will cause outer surface tension. The stress imposed upon the material due to heating or cooling is determined by equation 3.8. This stress can easily exceed the ultimate tensile strength of some ceramics and cause catastrophic failure. As stated earlier, no material is perfect; rather, they are all imperfect and have flaws in their micro-structure. Any crack or imperfection weakens the ability of the material to withstand an applied stress. These cracks and imperfections, or flaws, are generally the locations of first propagation of failure. If the average material flaw size can be determined by some non-destructive method, a critical temperature difference, ΔT_c, can be defined,

$$\Delta T_c = \frac{K_{Ic}(1-\mu)}{\alpha E \sqrt{c_i}} \qquad 3.9$$

where K_{Ic} is the fracture toughness, and c_i is the average flaw size. If the actual temperature difference is greater than ΔT_c, then the energy that develops in the material is greater than what the material can withstand, and cracks will grow until failure occurs.

Hardness: Hardness is a measure of a material's resistance to penetration of its surface by a hard object. Numerous tests determine hardness, and values vary according to the test but are used primarily for comparative purposes only. Specific hardness tests

are Brinell (HB), Rockwell (HR), Vickers (HV), and Knoop (HK). The Vickers and Knoop methods are considered micro-hardness tests because they form such small indentations that a microscope must be used to determine the necessary measurement. The Vickers micro-hardness test is used for the hardest materials and uses the least amount of load to achieve the indentation, and, therefore, is the main test used for ceramic materials. The reason hardness is a desirable feature with ceramics is that hardness correlates well with wear resistance, both mechanical and chemical. Chemical resistance is another important feature when considering ceramics for heat exchangers. With high chemical resistance, even at elevated temperatures, ceramics are ideal for industrial heat exchangers that use chemical fluids, which normally degrade a typical (non-ceramic) heat exchanger.

3.5 Processing Methods

Crystalline ceramics are manufactured into products by producing a shape comprised of the raw material from a fine powder. Traditional ceramic powders are mixed with water and shaped into the desired form. Advanced ceramics, on the other hand, do not possess the plasticity and formability that traditional ceramics do, and therefore must use different ingredients to achieve the desired shapes. The scope of this research focused on the advanced ceramics considering their use in heat exchange processes. There are four steps in the manufacturing sequence for these advanced ceramics: material preparation, shaping, sintering, and finishing.

Material preparation: The process of attaining the fine powders used in the shaping process is known as material preparation. Strength specifications in advanced

ceramics are usually much higher than in traditional ceramics. Since strength is inversely proportional to grain size, and size homogeneity is also important, a very fine powder is desired for the initial starting material.

Mechanical methods, or communition techniques, used for traditional ceramic material preparation, such as crushing and grinding, can be used to reduce the size of the material. Crushing reduces the raw material to smaller and smaller particles, while grinding then reduces these small particles to an even smaller size or powder. Unfortunately, many advanced ceramics have extremely high hardness values that can approach the toughness of the crushing and grinding materials. Any contamination from the grinding materials with the desired ceramic materials will reduce the purity and strength of the final product and affect other properties by introducing flaws into the micro-structure. These flaws cause stress concentrations that enhance the applied stress placed on a material.

Chemical methods for powder preparation create a better control on the homogeneity and purity of the raw material powder. Two common methods are freeze-drying and precipitation from solution. The freeze-drying technique involves dissolving the appropriate salt in water. The solution is then sprayed into small droplets that are rapidly frozen. Because the frozen particle includes some water molecules, the freeze-dried salt is placed in a vacuum chamber to remove the moisture. Once the moisture is removed, the salt is heated to decompose into the desired ceramic powder.

Precipitation from solution is another method for preparing new ceramics. This process begins by dissolving the desired ceramic compound from the initial mineral to remove and filter out impurities. Then, an intermediate compound is precipitated from

solution. The precipitates are then converted into the desired compound by heating.

In addition to the powders themselves, additives are introduced into the powders to help in the second step of the manufacturing process (shaping). Plasticizers, binders, wetting agents, deflocculants, and lubricants are common additives during the material preparation process. Plasticizers are added to improve the powder's plasticity and workability; binders help bond the ceramic particles into a solid mass in the final product; wetting agents aid in the powder's mixing ability; deflocculants help prevent clumping and premature bonding of the powders; and lubricants reduce the friction during the shaping and ease the process of product removal from the mold.

Shaping and sintering: The processes of shaping and sintering new ceramics are similar to the techniques involved in powder metallurgy and traditional ceramics. The two processes can be carried out simultaneously or independently, depending on the process. Sintering plays a slightly different role in the production of new ceramics compared to traditional ceramics. Since advanced ceramics normally do not involve the addition of water, sintering is required only to obtain the maximum strength and hardness. Sintering bonds individual grains into a solid mass, increases the density to approach the theoretical density, and reduces or eliminates porosity. Sintering is the process of heating the ceramic to approximately 80% to 90% of the melting temperature. When sintering is applied to the new ceramic, mass diffusion takes place across the contacting particle surfaces, accompanied by a small amount of plastic flow. This type of sintering is called solid state sintering because there is no liquid present. Solid state sintering causes the particle centers to move closer together, resulting in material densification, and can approach up to 98 % of the theoretical density. Sintering is a

permanent chemical and physical change process.

Hot pressing is a method that combines the shaping and sintering processes. Pressing compacts the starting powders through pressure by a large force on a particular die set. Hot pressing introduces elevated temperatures to the pressing process, allowing sintering to occur simultaneously with the formation of the ceramic. The combination of the processes results in densities that more closely approach theoretical densities and in finer grain sizes. An important drawback is the life of the shaping dies, which is reduced due to friction on the die surfaces from hot abrasive particles.

Isostatic pressing is an independent shaping method that involves uniform hydrostatic pressure from every direction on the entire surface area of the specimen. This process creates the most uniform, homogenous, green (un-sintered) product of all the shaping and pressing mechanisms, and since uniformity and homogeneity are desired features, this is an important shaping process.

A process for creating thin sheets of ceramic material is called the doctor-blade process. A common application of ceramic sheets is in the electronics industry where a ceramic sheet is used as a substrate material for integrated circuits. The doctor-blade process involves a ceramic slurry containment device that rests on a moving carrier film. One side of the container has a slit opening to allow the ceramic slurry an exit from the container as the carrier film moves. A wiper, called the doctor blade, determines the thickness of the opening slit. As the film travels through the drying zone, it becomes a flexible green ceramic tape that is then wound up on the take-up reel for further processing. While green, the tape can be stored in its roll form until further processing is desired before sintering to complete the final product. This ceramic processing

technique, at first glance, is not involved with heat exchangers, but as electronics advance and continue to shrink in size, the associated heat flux skyrockets. The ceramic layer must be involved with some type of heat transfer that is crucial to the life and performance of the circuit. Current research is investigating this need.

Another shaping process taken from powder metallurgy is powder injection molding. In this process, a ceramic powder is mixed with a thermoplastic polymer to provide adequate flow properties. It is then heated and injected into a mold cavity. Once cooled, the polymer is hard and holds the shape of the specimen. Although the process is performed under heating conditions, the ceramic specimen is not sintered because the temperatures required to plasticize the polymer are not close to sintering temperatures. Polymers have a much lower melting point than do ceramics and do not approach the 80 - 90% temperature level required in sintering. The now-green ceramic must have the polymer removed by a combination of thermal and solvent treatments known as debinding. Debinding must be carried out before sintering can occur. Although the process works for ceramics, it is not widely used. Difficulties in debinding and sintering and the reduced strength of the green ceramic post-debinding reduce the effectiveness of this process. Warping, cracking, and other micro-structural flaws are inherent in this manufacturing process.

Finishing: The final operation for any manufacturing process is finishing. In the case of ceramic manufacturing, finishing achieves obvious purposes. Finishing can involve an increase in dimensional accuracy, an improvement in surface finish, and/or minor modifications in the part geometry. Most finishing operations usually use processes that involve grinding or other abrasive means such as honing, lapping,

polishing, and buffing. With hardened ceramics, diamond is the abrasive material of choice since its hardness exceeds that of all ceramic materials.

3.6 Transition of Material to Current Research

The ceramic material research completed, described here, allowed for a more knowledgeable choice of material and better understanding of difficulties when they were encountered. Figures 3.1 and 3.2 depict two specific properties of interest to this research. The properties are shown compared to those of copper, one of the more typical materials used in metallic heat exchangers. Aluminum Nitride was chosen for the base material of a ceramic plate heat exchanger concept, as explained in detail and defended in chapter 4. The test section incorporated a single plate to separate two fluids in a counter-flow configuration. The plate was shaped and sintered with grooves on both sides to allow for the fluid flow. More detailed explanations and drawings of the ceramic test section are given in chapter 4.

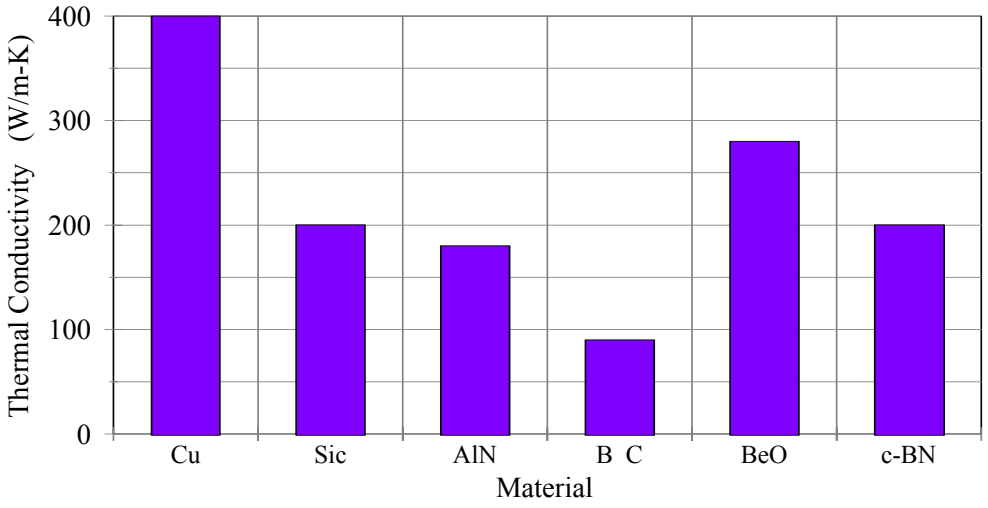

Figure 3.1 Thermal Conductivity of Selected Ceramics vs. Copper (for comparitive purposes)

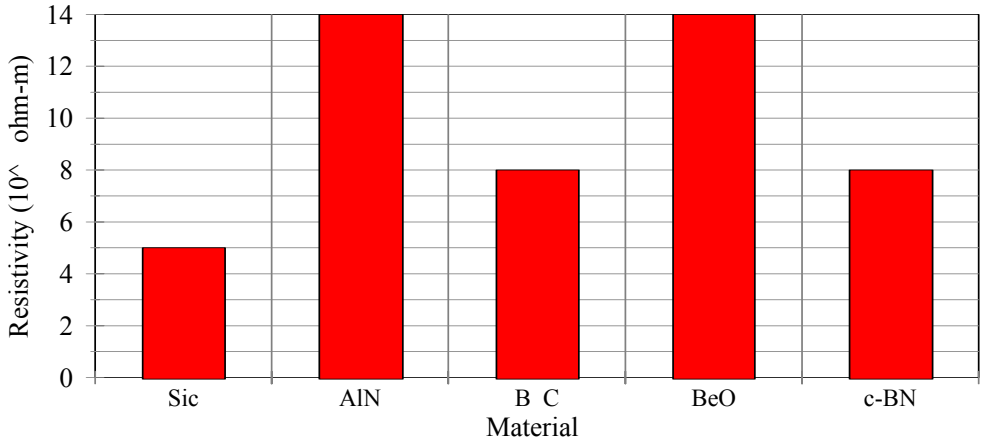

Figure 3.2 Electrical Resistivity of Selected Ceramics

Chapter 4

EXPERIMENTAL APPARATUS AND PROCEDURE

4.1 Introduction

This chapter describes the experimental apparatus and procedure involved in the present study. The setup is a dual loop designed for the heat exchanger incorporating a counter-flow pattern. The heat exchanger designs are also discussed in addition to the loops to which they are connected. The setup is split up into two loops and will be described in order as:

a. Primary Loop, and

b. Secondary Loop.

Details of each portion of the dual loop and each test section are discussed fully in the following sections.

4.2 Experimental Setup

The schematic of the entire apparatus, both the primary and secondary loops, is shown in figure 4.1. The primary loop travels through either the shell of the 5-port metallic heat exchanger and fluid flow field, or the upper portion of the ceramic heat exchanger. The secondary loop travels through either the tube bundle of the 5-port metallic heat exchanger, or the lower portion of the ceramic heat exchanger and the corresponding flow field.

4.2.1 The Primary Loop The primary loop can be used for refrigerant, in this case R-134a, or a single phase fluid. The primary loop consists of a condenser, a sub-cooler, a pump, a flow-meter and sensor, a pre-heater, a filter-dryer, and a differential

pressure transducer. The condenser is used either to maintain system pressure when used with a refrigerant, or help regulate system temperature when used with a single phase fluid. The sub-cooler is a simple R-12 cooling loop to ensure sub-cooled liquid flow to the pump and flow meter when used with a refrigerant, or boost the system's cooling performance when used with a single phase fluid. Thermocouples are located at each port entering and leaving the test section area, as seen in figure 4.1 test section area. At each of the two locations, two thermocouples are placed inside a sealed stainless steel, small diameter tube. These thermocouple probes are inserted into the flow to determine average inlet and outlet fluid temperatures. These temperature locations can provide verification of saturation conditions when used with a refrigerant, as well as determination of single phase temperature dependent inlet properties. Although not a part of the loop itself, a high voltage power supply can be connected to the actual heat exchanger/test section to establish an electric field in the primary loop's fluid flow field during testing incorporating the EHD enhancement technique. Tests involved with the five-port metallic HX did not incorporate this power supply, as the design did not allow for a voltage connection to produce an electric field in the tube bundle, or refrigerant flow. The connections for the ceramic HX are described in sections 4.4, and depicted in greater detail in figures 4.7 - 4.9.

4.2.2 The Secondary Loop The secondary loop is used for a single phase liquid, in this case Polyalphaolefin, PAO, a synthetic oil used in aircraft avionics cooling, or JP8, aircraft fuel, both displaying thermophysical properties that are highly dependent on temperature, as shown in Appendix A. The secondary loop simply consists of a pump, a filter dryer, a heater, and a differential pressure transducer. A high voltage

power supply can also be connected to establish an additional electric field in the secondary loop's fluid flow field. This power supply and the one used in the primary loop are independent of each other and are controlled separately to adjust the electric field intensities in each flow. Tests involved with the 5-port metallic heat exchanger used this power supply to provide the EHD field on the shell side of the HX, while the ceramic heat exchanger was setup to use one, or both, power supplies.

The secondary loop can only be used as the hot fluid. A 900 watt coiled loop electrical resistance heater is used as the heat source for the entire double loop system. The thermocouple arrangement is identical to that in the primary loop. The set of thermocouple probes coupled with the primary loop's set of thermocouple probes are used to determine the logarithmic mean temperature difference across the test section, and ultimately the overall heat transfer coefficient, U.

One, or two, high voltage power supply is used for the setup, but not necessarily an integral part of either loop. Each loop can operate with or without the applied EHD field, as is the scenario involved when attaining base case conditions. The power supplies can be used to establish an electric field in each loop's fluid flow field. These voltage connections are discussed in each heat exchanger's test section description.

4.3 Five-Port Metallic Heat Exchanger

The 5-port metallic heat exchanger is an actual, real-size, working heat exchanger in a complete unit. The HX is of a shell and tube bundle configuration shown in figures 4.3 and 4.4. The shell is of stainless steel tube with inside diameter of 0.652 in. (0.0166 m) and length of 6.3 in. (0.16 m). The tube bundle is constructed using 19 stainless steel

tubes, each with an outside diameter of 0.0625 in. (0.0016 m) and inside diameter of 0.0545 in. (0.0014 m) The bundle is held in place in the configuration shown in figure 4.4 by two Teflon bundle caps. The tubes marked on the figure are connected together by thin wire threaded through machined channels in one of the bundle caps. These are then connected to the voltage source through the contact connection of the top tube, in the arrangement shown in Fig. 4.4. This contact connection is considered the 5^{th} port. The unmarked tubes are similarly connected in the opposite bundle cap and connected to ground. This electrical design, one in which the actual tubes serve as electrodes, actually simplifies the technology in that no additional electrode insertion need configured and engineered. The arrangement of alternating charged and grounded tubes allows for the greatest inhomogeneity in the bulk flow through the secondary loop containing either PAO or JP8. According to the governing EHD equation found in chapter 2, the third term signifying the electrostrictive force component deals with inhomogeneities in the electric field. The configuration represented allows for the most significant variation of intensities and direction of the electric field when compared to other arrangements considered. The first ring of tubes outside of the center tube are of identical charge, otherwise, if this ring were alternately connected similar to the outer ring, the only electric field produced would be between neighboring tubes in each ring, rather than between rings in addition to between neighboring tubes.

4.4 Ceramic Heat Exchanger Test Section

The test section incorporates the ceramic heat exchanger and the frame in which it is housed. The test section frame's primary purpose is to seal the heat exchanger to

prevent cross-contamination between the two fluids that are transferring heat. This setup uses a counter-flow configuration; the two fluids are flowing parallel to each other, but 180° apart in flow direction. The frame also holds the charged electrodes to which high voltage for each flow field is supplied. Figures 4.5 through 4.9 show the test section in more detail.

Ceramics, because of their low density and potential promise to the aerospace industry, were researched to find those with favorable properties. This research has been presented in the previous chapter. The first properties investigated were thermal conductivity and electrical resistivity. Electrical resistivity is the property that portrays the material's ability to resist electrical flow. Most ceramics that have fairly high thermal conductivities also have low electrical resistivities. A handful of ceramics displays both properties as favorable to the current application. In addition to these two important properties, it was essential to look at other properties as well. Density is important to reduce the component's overall weight. Thermal expansion must be fairly low for changes in fluid and environmental temperature gradients. A high value for thermal expansion can lead to thermal shock failure. Thermal shock will cause catastrophic failure if the material is not chosen wisely. Hardness can also be important because a material's hardness is directly related to its mechanical and chemical resistance. Table 4.1 lists certain ceramics with selected thermo-mechanical properties.

Table 4.1 Thermo-Mechanical Properties

Material	Density (g/cm^3)	Expansion ($10^{-6}/K$)	Conductivity (W/m-K)	Hardness (kg/mm^2)	Resistivity (ohm - m)	Modulus (GPa)
SiC	3.10	4.50	200	2600	10^5	500
AlN	3.25	5.00	180	1100	10^{14}	331
B_4C	2.45	5.60	90	3200	10^8	450
BeO	2.86	8.50	280	1200	10^{14}	400
c-BN	3.49	4.80	200-900	2000	10^8	450

As seen in table 4.1, Silicon Carbide (SiC) has low density, the lowest thermal expansion coefficient of those listed, a decent thermal conductivity, and high hardness; but, the electrical resistivity is the lowest shown and elastic modulus is the highest of those shown. Considering the importance of electrical resistivity for the current application, SiC was ruled out. Tetra Boron Carbide (B_4C) has excellent hardness and a very low density, but the thermal conductivity was the lowest. Beryllium Oxide shows very good promise even though the thermal expansion coefficient is fairly high. Its electrical resistivity and thermal conductivity are very suitable to the present application, but an important drawback is the manufacturing aspect of using this material. Considering that Beryllium is toxic, the cost would be high due to the extra care needed during manufacturing. Cubic Boron Nitride (c-BN) has excellent potential due to its thermal conductivity but a lower electrical resistivity. Aluminum Nitride (AlN) was chosen for its excellent electrical resistivity value and decent thermal conductivity. Although the thermal conductivity is important, the relative closeness of the values does not contribute a significant difference due to the small thickness of the material through which the heat is being transferred.

Once the material was chosen, the next obvious step was to design the heat exchanger to fit the requirements. A sub-compact geometry was desired; therefore a β of greater than 2500 m^2/m^3 (761 ft^2/ft^3) was needed. Most of the design iterations for this module dealt with targeting a fairly simple geometry while still achieving the appropriate sub-compact area density. Figures 4.5 and 4.6 show the final design. The piece has finished dimensions of 26.75 mm x 126 mm x 4.5 mm (1.05 x 4.96 x .177 in.) The actual dimensions of the channel area are 22.75 mm x 120 mm x 1.5 mm (.896 x 4.72 x .059 in.). There are eight channels on one side and nine on the opposite side to allow for a ½ channel offset through the thickness for additional strength. Each channel has its maximum dimension of 2.23 mm (.068 in.) with a face angle of 60 °. There is a ledge around the entire perimeter to allow for a gasket for sealing purposes. The gasket material is manufactured using SBR, styrene butadiene rubber, and is compatible with the fluids being used.

With the use of EHD, an electrical circuit must be incorporated in the test section to create an electrical field in the flow. A plate electrode is placed on top of the channels and is connected to the high voltage power supply through the voltage port in the test section frame (see figure 4.8.) The ground electrode had to be designed to lie at the bottom of the channels. This was accomplished by placing a silver layer coating at the bottom of each of the channels. This silver coating and the ceramic test section was then baked at a temperature of 550 °C, high enough to cure the silver and bond with the ceramic. Figures 4.7 – 4.9 show greater detail for the connections of the high voltage and ground source. A thin sheet of brass is wrapped around one end of the ceramic piece and is held in place once the frame is assembled. This brass is connected to a ground source

to complete the connection. Figure 4.8 shows one half of the frame with one of the two fluid ports. A second identical frame piece is used to sandwich the ceramic test section resulting in the test section with each side as part of each of the primary and secondary loops.

4.5 Experimental Procedure

4.5.1 Equilibrium With either of the two test sections, five-port or ceramic, it is necessary to establish equilibrium under base conditions before any data can be taken or high voltage introduced. Initially, all systems in both the primary and secondary loops are indexed on. This includes pumps, sub-cooler, condenser loop, and heaters. The pumps for each loop were connected to a variable current device so that each fluid medium was adjusted to the desired Reynolds number, Re. As can be seen in figure 4.1, the dual loop schematic, the secondary loop does not include a flowmeter. Mass flux is calculated through typical heat transfer equations, mainly $Q = \dot{m} C_p \Delta T$. The $\dot{m}$ can be calculated because all other values are known, as shown in this chapter's data reduction section. The specific heat is known at the inlet according to property relations shown in Appendix A, ΔT is known by temperature measurements before and after the test section, and the heat flux is determined by the secondary loop's heater and known heat transfer area of each test section. Following, Re can be determined by:

$$\mathrm{Re} = \frac{\rho u D}{\mu} \quad \Rightarrow \quad \frac{\rho u A D}{A \mu} \quad \Rightarrow \quad \frac{4 \dot{m}}{\pi D \mu} \tag{4.1}$$

The equivalent hydraulic diameter is used in place of D for both the five-port metallic and ceramic HXs. As discussed in an earlier section, the secondary loop is always the

hot loop and therefore, the heater voltage is also adjusted by another variable current device to establish the required heat flux introduced into the system. The primary loop using R-134a is sub-cooled to allow more accurate flow measurement at the flowmeter. The pre-heater is also adjusted by a variable current device to establish the desired condition of refrigerant quality. The temperature and pressure are known prior to the pre-heater and thus, the enthalpy. Refrigerant quality can be determined by knowing how much heat is input through the pre-heater, and likewise knowing what quality is desired, the pre-heater voltage can be determined. The heat input is calculated by knowing the voltage input with the measured resistance of the heater coil. The test section is sufficiently insulated and any heat leaks are within the uncertainty values.

As the system is operating and components are adjusted to meet desired parameters, both systems are changing temperature. As the temperature of each fluid changes, the Reynolds number also changes due to the dependency on density and viscosity, which are both functions of temperature. Therefore, while attaining equilibrium at base case conditions (described below), many components must be adjusted while continually determining and calculating the necessary parameters.

4.5.2 Base Case Conditions Once a base case condition is set, that is, equilibrium has been reached with operating parameters verified, data can be recorded. Base cases are experiments of varying operating parameters with zero applied EHD voltage. In other words, every experimental set has a base case associated with it. Additionally, there is a master base case, that from which all base case conditions are varied. Table 4.2 gives the master base cases for each HX.

Table 4.2 Master Base Cases

Operating Parameter	**Five-port Metallic HX**	**Ceramic HX Test Section**
Re (primary)	1000 (refrigerant – tube side)	500 (refrigerant)
Refrigerant Quality	15%	30%
Refrigerant T_sat	20 °C	20 °C
Re (secondary)	250 (oil-fuel – shell side)	500 (oil-fuel)
Heat Flux	25 kW/m²	5 kW/m² (based on both sides)

Three sub-cooled refrigerant temperatures are averaged, along with the refrigerant pressure to determine conditions prior to the pre-heater. The refrigerant's pre-heater voltage is used to verify refrigerant quality as the fluid enters the test section. Each inlet and outlet port of the test section houses two thermocouples and these are averaged to determine the logarithmic mean temperature difference, or LMTD. The mass flow rate of the secondary fluid is calculated using averaged temperature measurements at locations prior to pump and after the heater. Both the heater and the secondary pump must be added together to determine heat input for mass flow calculations. Once the mass flow is determined, this value is coupled with the known secondary fluid's specific heat value, and test section's inlet and outlet temperatures to determine the rate of heat transfer through the test section. Finally, the overall heat transfer coefficient, U, can be calculated since the test section's heat transfer area is already known. See Appendix B for sample data sheet and section 4.6 for the calculation flow. Additionally, Appendix C includes the error analysis for the experimental data.

4.5.3 Non Base Case (EHD field applied) Experiments The previous section's determination of base case conditions is very important, in that the validity of EHD depends on the accuracy of these base case conditions. Once equilibrium was reached for base case and data tabulated, the high voltage supply was switched on and adjusted to a predetermined level. [This level, and subsequent incremental levels, was based on an I-V (current vs Voltage) characteristics curve test performed ahead of the experiments. This test simply determined how high the voltage could be increased to and the level at which enhancement would begin. Each fluid and electrode configuration has its own maximum capacity of field intensity before breakdown. This breakdown of the fluid results in a spark, a result of the current expended directly through the fluid, and a spike in corresponding current. It is at this voltage level, the spark over limit, which limits further increases in voltage. The fluid's electrical resistivity has been exceeded and can no longer hold the applied voltage. The electrical configuration of each HX is, in essence, an electrical circuit. As voltage increases, the current traveling through the circuit also increases. Additionally, due to the power supplied is DC current, the efficiency is quite high, and very little voltage is lost during transfer. Under most circumstances, the current does not rise significantly until a certain level of voltage. This level is typically a good indication that the applied voltage is producing movement in the fluid, and can be the onset of possible heat transfer enhancement.] As each incremental voltage is met, the system is allowed to reach equilibrium once again. As voltage is introduced, temperatures change at the test section ports. As the temperature values cease to change, equilibrium has been attained, and the same values are again recorded. After each recordation, voltage is increased to the next incremental level and the

procedure repeats until the maximum voltage (predetermined level prior to the spark over limit) is met and the test is completed.

While voltage is increasing past the onset level, the system's ability to transfer heat is increased. This increased heat transfer changes the temperatures and/or quality of the fluids. As stated earlier, some of the operating parameters, namely Re, will change accordingly due to these temperature changes. Due to the expected application of this technique for being on-demand, the pump power is not adjusted, rather it is held constant to maintain the initial mass flux conditions.

4.6 Data Reduction

Experimental data was transferred to a computerized spreadsheet with cell formulas to determine the desired and necessary quantities. A cut and pasted sample sheet is shown in Appendix B, copied from one of the test runs. Data reduction analysis follows.

4.6.1 Determination of Desired Test Conditions The first set of temperatures, listed as T_a, T_b, and T_c on Appendix B's spreadsheet, are averaged to get a sub-cooled refrigerant temperature, T_{sub}. This value, coupled with the average Ref $_{in}$, refrigerant flow rate, and known liquid specific heat, yields the amount of heat required by the refrigerant pre-heater to bring the refrigerant to saturated conditions, or the quality, X, equal to zero, through the following standard equation.

$$Q = \dot{m} Cp_l \left(T_{sat} - T_{sub}\right) \qquad 4.2$$

The refrigerant pre-heater incorporates a variac to adjust the voltage input. This known voltage, and the measurement of the heater's resistance yields Q_{phtr}. An

adjustment of the variac greater than that required above will not affect temperatures, but only increase the quality at the inlet of the test section. The realization that the increase in the pre-heater's voltage does not increase Ref_{in} shows that the refrigerant is in two-phase at that point and it follows that decreasing the voltage will reduce the quality to any desired value, and vice-versa. To maintain a desired average test section refrigerant quality while the heat flux varies requires the manipulation of the pre-heater. Conditions of lower heat flux through the test section require a higher inlet quality such that the outlet quality yields an average of which matches the desired conditions. Knowing $T_{sat,}$ system pressure (regulated by the external chiller temperature), tabulated saturation and vaporization enthalpies, h_f and h_{fg}, the enthalpy at the inlet of the test section can be calculated by:

$$h_{in} = X_{in}\, h_{fg} + h_f \tag{4.3}$$

Subtracting the Q needed to get x=0 from Q_{in}, which is the heat supplied to the secondary loop that is being removed by the primary loop through the heat exchanger test section, will yield an exit quality determined by the following formula:

$$h_{out} = h_{in} + \frac{Q_{in}}{\dot{m}} \tag{4.4}$$

With inlet and outlet enthalpies calculated, the exit quality can be determined:

$$X_{out} = \frac{h_{out} - h_{sat}}{h_{fg}} \tag{4.5}$$

4.6.2 Determination of the Overall Heat Transfer Coefficient

The single phase fluids in use for this study, namely PAO and JP-8, have a temperature dependent property of specific heat. This relation is linear and constructed using a straight line best fit equation from manufacturer's provided data as shown in appendix A. The heat input, Q_{in}, determined from the fluid's heater and pump power, combined with the temperature sensitive value of the specific heat, Cp, and the pump inlet and first set of test section inlet temperatures (used as T_{out} for the pump/heater combination), yields the mass flux of the hot side, single-phase, fluid:

$$Q_{in} = \dot{m} Cp \left(T_{in} - T_{out}\right) \tag{4.6}$$

This portion of the procedure takes patience to reach equilibrium and desired conditions. For every adjustment of the mass flux, the test section temperatures change. These changes can have a pronounced effect on Cp, thereby requiring constant calculations and subsequent pump adjustments to maintain the required Reynolds number for the secondary loop flow.

Once the mass flux and heat input, $Q_{in,}$ are set, in addition to the primary loop being stable, the actual heat transferred through the test section can be calculated using equation 4.6 and the test section inlet and outlet temperatures rather than the temperatures used to determine the mass flux.

The overall heat transfer coefficient requires the LMTD, or logarithmic mean temperature difference of the inlet and outlet temperatures of both the single-phase, hot side liquid, and the refrigerant:

$$LMTD = \frac{\left(T_{hot-in} - T_{cold-out}\right) - \left(T_{hot-out} - T_{cold-in}\right)}{\ln\left[\frac{\left(T_{hot-in} - T_{cold-out}\right)}{\left(T_{hot-out} - T_{cold-in}\right)}\right]} \quad 4.7$$

Once LMTD is calculated, the overall heat transfer coefficient is determined by:

$$U = \frac{Q}{A\ LMTD} \quad 4.8$$

where Q is the heat transferred via the test section and A is the designed heat transfer surface area.

4.6.3 Determination of EHD Enhancement Values The previous analysis of the overall heat transfer coefficient, U, is used for every test run for this study. With zero applied voltage, the U determined is signified as the U_{base} for the specific conditional set. For subsequent test runs for each set, the high voltage power supply is adjusted incrementally to set values, allowed to reach equilibrium, and data is then tabulated once again and a U value is found for a second set of identical conditions with the exception that high voltage is held across the fluid medium. Voltage and current readings are recorded, tabulated, and converted to kV and mA through the appropriate unit conversions specific to the power supply and measuring apparatus. The typical increment adjustments are 3 kV. EHD enhancement is subsequently:

$$\frac{U}{U_o} = \frac{U_{V\ applied}}{U_{base\ case}} \quad 4.9$$

The power requirement necessary to gain any enhancement in U is found by:

$$P_{EHD} = V_{EHD}\ I_{EHD} \quad 4.10$$

The power ratio, α, is then determined as a percentage of the heat input to the test section, Q_{in}, which is the combination of the heat input by the heater and the pump:

$$\alpha = \frac{P_{EHD}}{Q_{HTR} + Q_{pump}} \times 100\% \qquad 4.11$$

The corresponding pressure drop due to the enhancement is found through a differential pressure transducer with pressure ports on inlet and outlet sides of the test section. The pressure drop increase, γ, is found by:

$$\gamma = \frac{DP_{V\ applied}}{DP_{base\ case}} \qquad 4.12$$

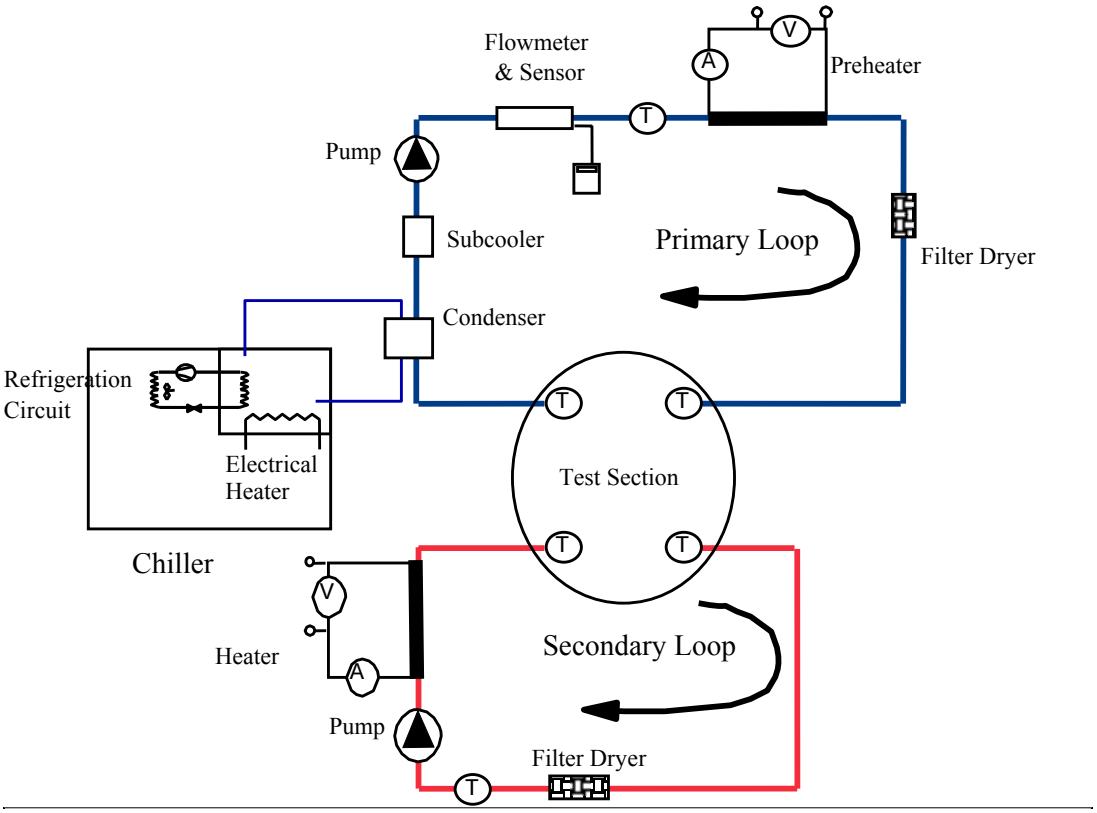

Figure 4.1 Schematic of Dual Test Loop

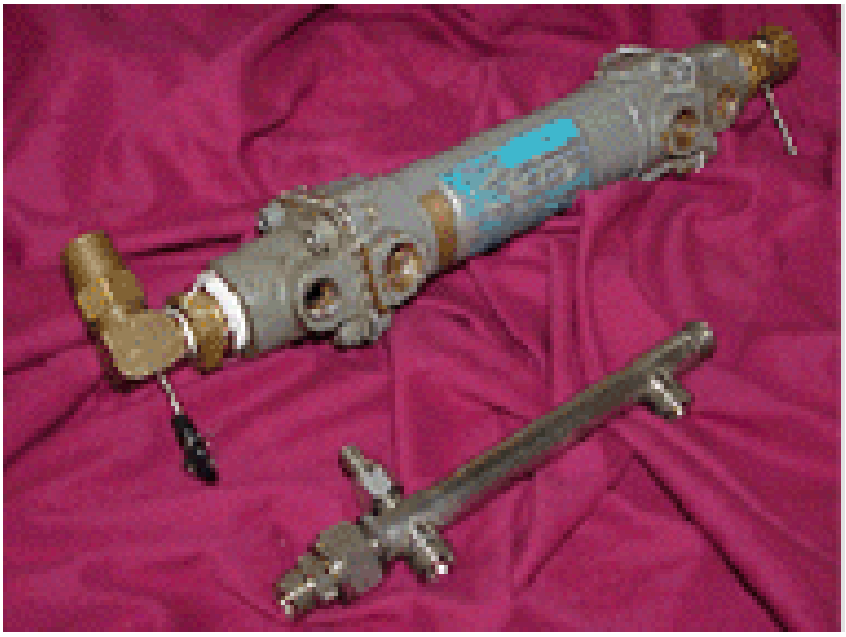

Figure 4.2 Five-port Metallic Heat Exchanger – pictured with a typical shell and tube heat exchanger of comparable capacity

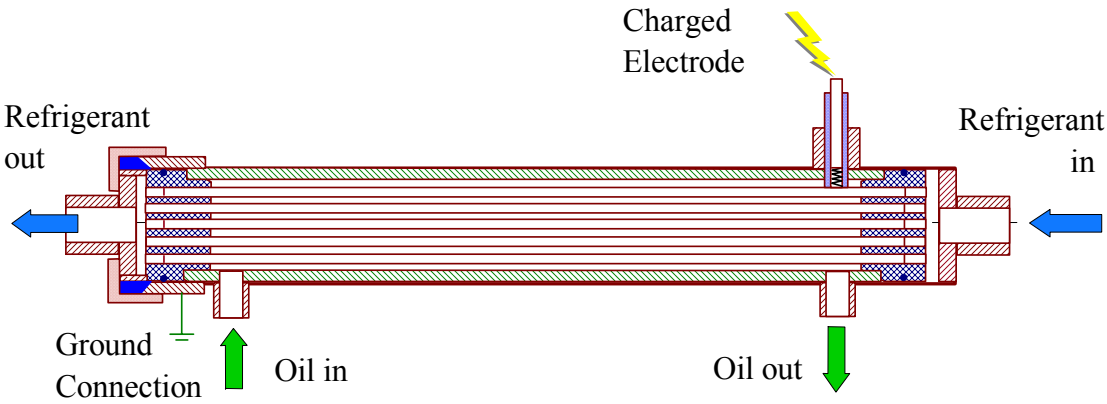

Figure 4.3 Five-port Metallic Heat Exchanger

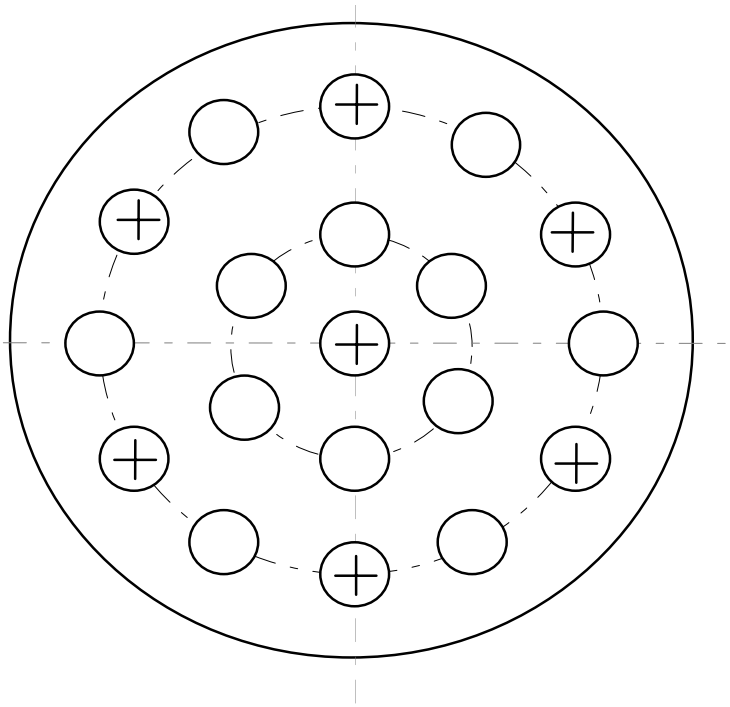

Figure 4.4 Tube bundle configuration

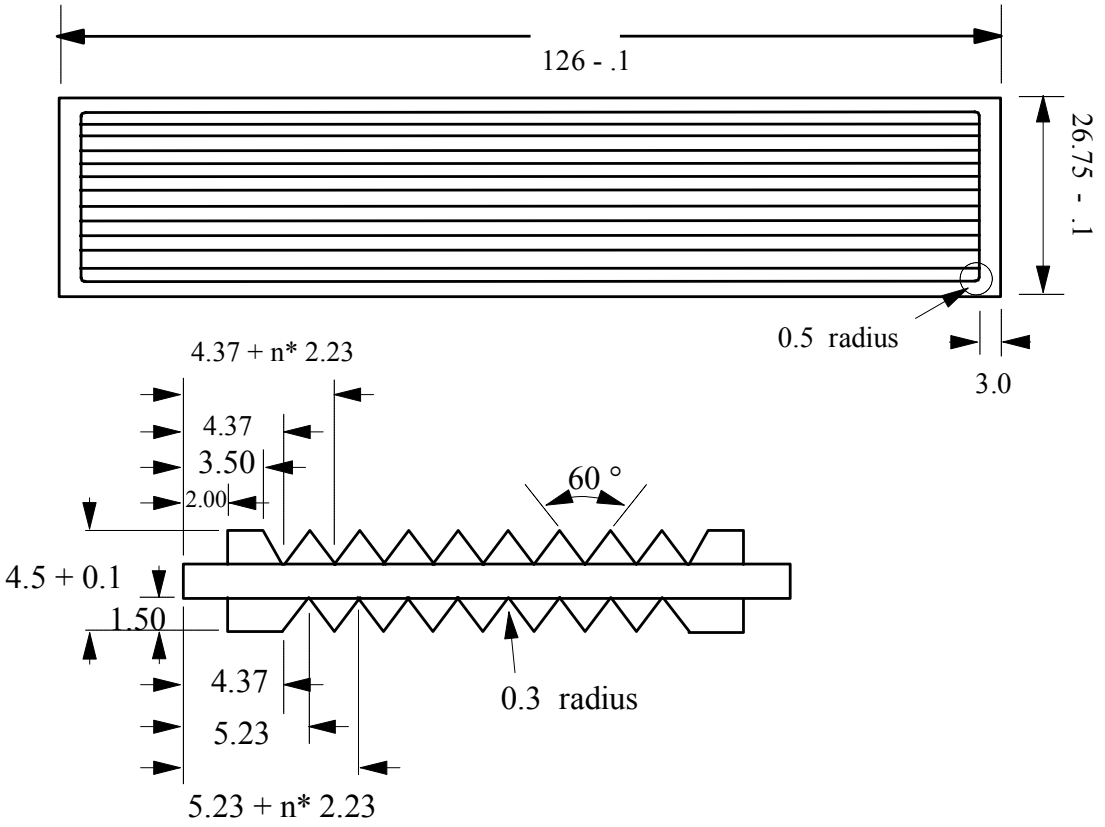

All dimensions are in mm, and not necessarily to scale.
The piece has 9 channels on the top and 8 channels on the bottom. (channels have similar geometry)

n in the dimension equation represents the channel number counted from the measurement base line

4.5 Dimensional Drawing of Ceramic HX Test Section

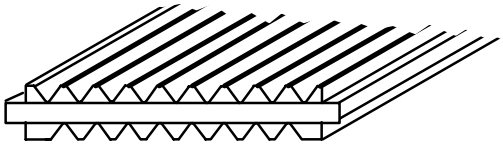

4.6 3-D View of Single plate Ceramic HX

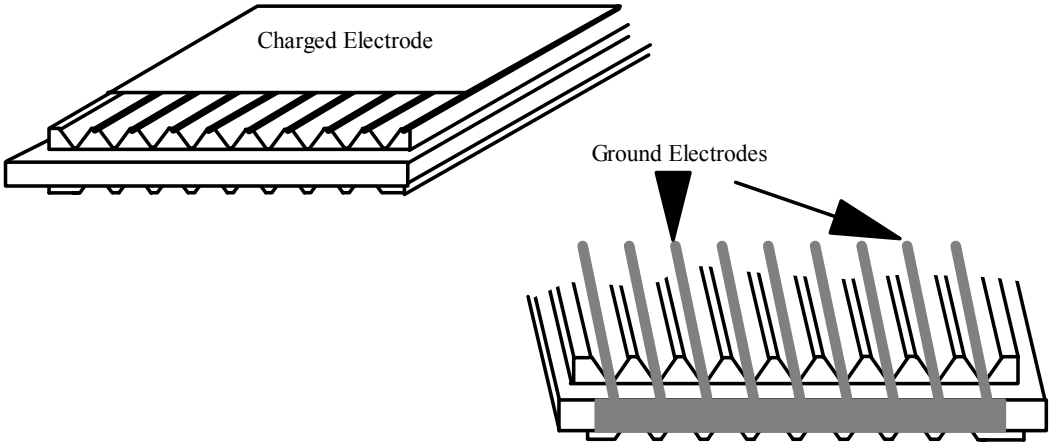

4.7 High Voltage and Ground Connections

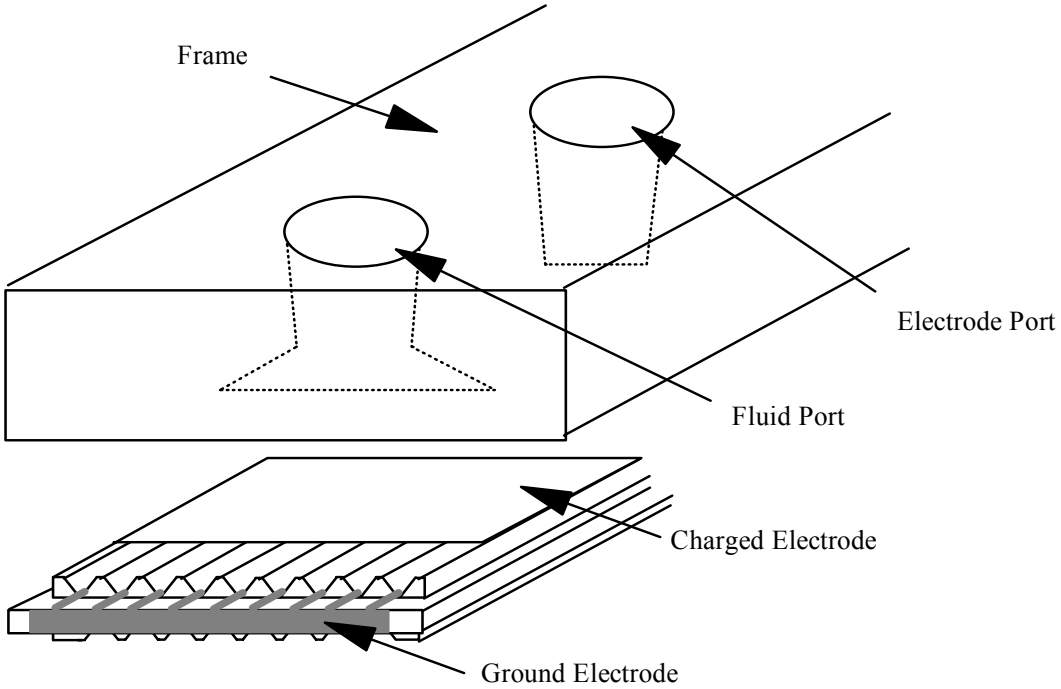

Figure 4.8 Ceramic Test Section with Frame

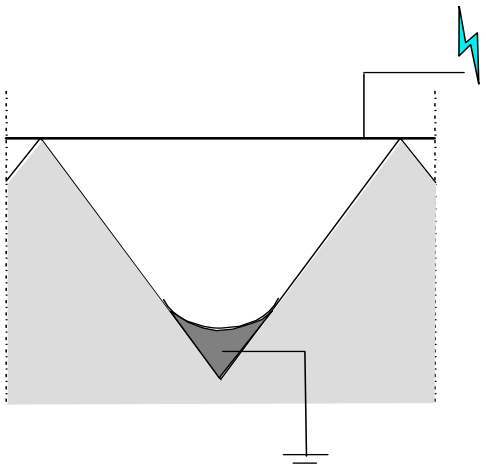

Figure 4.9 Ceramic single channel electrode configuration

Chapter 5

RESULTS & DISCUSSION

5.1 Introduction

This chapter presents results and discussions of the experimental data for the heat exchanger enhancement studies on the five-port metallic and ceramic heat exchangers. The presentation is given in two parts. Part I will discuss results of the five-port metallic, EHD-enhanced shell-and-tube heat exchanger and part II of the chapter will discuss the results obtained with the ceramic heat exchanger. In each part, results for a base case (absence of EHD field) are discussed first and are followed by an EHD-enhanced case, where the effect of an applied EHD field on performance improvement of the base case is discussed. A summary of the results obtained and the analysis is given at the end of this chapter.

5.2 Five Port Shell & Tube Bundle HX

The five-port, shell and tube bundle HX produced rather encouraging enhancement results on the overall heat transfer coefficient. R-134a was the fluid moving through the tube side of the shell and tube bundle. Tubes were smooth inside and had no provisions for enhancement. Two different fluids were tested in the shell side: PAO and JP8. For tests using both PAO and JP8, increasing the voltage affected the Reynolds number on the shell side by reducing the average temperature of the secondary loop. As discussed in chapter 4 and shown in Appendix A, the kinematic viscosity of PAO is very temperature dependent. The enhanced heat transfer, while producing more

effective cooling of the PAO, produces a higher kinematic viscosity of the PAO strictly due to the reduced temperatures. Considering that kinematic viscosity is a variable in the equation for Reynolds number, the corresponding Re value, after voltage is applied, decreases. As discussed earlier in chapter 4, this resulting change in dimensionless operating parameters is not adjusted to maintain base conditions; rather the mass flux remains constant. One of the major selling points and expected applications of this technique is its on-demand feature. In other words, EHD can simply remove additional heat loads, above a certain design threshold, by increasing the applied voltage. No other adjustments to the cooling system are required to handle the increased load.

Typical trends of enhancement, power ratio, and pressure drop are depicted the 5-port metallic heat exchanger in figures 5.1 through 5.3, respectively, using R-134a in the tubes and PAO in the shell. Conditions of refrigerant Re and average quality of 1000 and 16%, respectively, PAO Re of 250, and a heat flux of 25 kW/m² (7925 Btu/hr-ft²) were used during testing and are stated in the figures. These conditions are also considered the master base case, as defined in chapter 4. Figure 5.1 relates the enhancement vs. voltage showing an enhancement onset occurring at 6 kV of applied voltage, with a maximum enhancement of about 2.3, corresponding to an overall heat transfer coefficient of 2134 W/m²-K. Uncertainty analysis is presented in Appendix C.

The enhancement ratio is simply the enhanced overall heat transfer coefficient divided by the base case, or zero applied voltage, overall heat transfer coefficient. Figure 5.2 depicts the ratio of supplied EHD power vs. the amount of heat being transferred. Power increases more drastically compared to the enhancement with which it is associated, although the maximum power requirement for these conditions is about

1.77%. As little as 1.8 % of the heat exchange rate was used to remove approximately 130% more heat. The power required to gain the enhanced heat transfer is calculated by multiplying the applied voltage with its corresponding current, as shown in chapter 4's Data Reduction section. Figure 5.3 illustrates the corresponding pressure drop for the same set of tests as shown in figures 5.1 and 5.2. At maximum enhancement, there is an equivalent increase in pressure drop due to the applied voltage, or about 2.4 times. Most passive enhancement techniques may increase the pressure drop across the heat exchanger, sometimes as much as four times for the given heat transfer rate or more compared to the values recorded with this type of enhancement. Figure 5.4 depicts performance variation of the overall heat transfer coefficient vs. applied voltage for the tube and shell sides, representing PAO and JP8 fluids, respectively, under identical operating conditions. As seen there, as the applied voltage increases the overall heat transfer coefficient increases. This is because with an increase in electric field intensity, the EHD-induced secondary motions are stronger, thus leading to increases in the heat transfer coefficients. PAO is found to have slightly better base case heat transfer characteristics, but JP8 displays a greater maximum enhancement.

Next, attention is brought to figures 5.5 and 5.6. Here, variation of heat flux on the base and EHD-enhanced cases are depicted. Corresponding power consumptions and pressure drop increases are shown as α and γ, respectively. As shown, heat transfer is minimally affected with varying heat fluxes during base case testing, but the overall heat transfer coefficient generally increased as heat flux increased with maximum applied EHD voltage. EHD is more effective due to a higher rate of applied heat. A general increase in enhancement is observed due to sharper gradients in fluid properties, in

addition to lower densities at higher temperatures allowing easier mixing. When comparing the two figures, PAO has shown to experience a maximum threshold due to its significantly higher kinematic viscosity. The high viscosity is competing against electric body force and may be blocking higher enhancement levels, whereas JP8, in figure 5.5, still can accept the increasing rate. Future testing should investigate higher heat fluxes to verify whether or not the enhancement levels experience a maximum at a certain amount of applied heat flux.

Figures 5.7 and 5.8 depict variation of the Reynolds number on the base and EHD-enhanced cases. As expected with increasing Re, these show a decrease in enhancement. Each point on the graph includes the associated enhancement level as U/U_o. It is an established fact that EHD works best with laminar flow. As the flow increases towards a turbulent flow regime, zero applied voltage scenarios already have increased mixing due to the naturally occurring eddy currents in the flow.

Finally, figures 5.9 and 5.10 show the lack of any significant trend with respect to changing refrigerant quality, although any enhancement could be hidden within the level of uncertainty. Uncertainty values for all tests varied between just below 7% and just over 8.5%.

There are some who question that the power supplied to gain the enhancement would not be better, or equally, served by redistributing the power to the pump, thereby increasing the mass flow resulting in a more natural enhancement. The pump affinity laws state that the ratio of pump power is equal to the ratio of the flow rates cubed. The approximate 2% power consumption would roughly double the pumping power, resulting in a 25% increased flow rate. This increase, if shown on figure 5.8, would lie within the

base case uncertainty error bar. Clearly, using the power to disturb the thermal boundary layer has much more significant dividends than applying the same power to increase the mass flux.

5.3 Ceramic Heat Exchanger

The research involved with the ceramic HX was challenging, exhaustive, and required painstaking care in assembling the heat exchanger and testing of it. Setbacks inherent with fabrication of this micro channel ceramic heat exchanger caused the project to surpass the time and money budget allocated towards the project, and disallowed concrete enhancement data from the effect of electric fields. However, successful base case data sets were collected and some of the difficulties encountered with the application of the electric field were solved, paving the way for future work. Prior to final failure, baseline data were taken using R-134a through the primary loop and PAO through the secondary loop. These tests all used a master base case of equal Reynolds numbers with a value of 500 for each fluid, an average oil temperature of 30ºC (86°F), a saturated liquid refrigerant temperature of 20ºC (68°F), an average refrigerant quality of 30 %, between inlet and outlet, and a heat flux of 5 kW/m² (1585 Btu/hr-ft²) based on an area that encompasses both sides of the ceramic plate.

Figure 5.11 depicts data of the overall heat transfer coefficient, U, determined through a range of varying PAO Reynolds numbers, from 350 to 1000. As expected, heat transfer is increased as flow regimes increase in Re. Figure 5.12 displays results of U over a range of refrigerant values of average quality, 20% to 47%. Similar base case results were shown for the 5-port metallic HX of no particular trend. Similar reasoning

could hold true in that any trends may be hidden within the level of uncertainty. Figure 5.13 shows the values of U for a range of refrigerant Reynolds numbers, 350 to 750. Again, heat transfer is increased as flow regimes increase in Re, and this trend follows expected results.

These three sets of data depict trends that are recognizable and expected. 1) Increasing Reynolds number yields higher heat transfer coefficients; and, 2) refrigerant quality has little effect on heat transfer. As quality increases, the amount of vapor increases and rises to the top of the channel. Only at higher quality levels would a flow be adversely affected, due to increased vapor quantities and lack of fluid wetting the heat transfer surface. Conversely, if the setup described in chapter 4 were reversed, in that the primary loop, with refrigerant, were configured so that it was on the bottom, noticeable decreasing heat transfer trends would occur due to vapor convection, rather than liquid convection.

The interesting aspect of the base case ceramic data is the fairly high values for the overall heat transfer coefficient. The method for determining U has been shown in chapter 4, and uses LMTD analysis. As discussed in earlier chapters, higher area densities produce greater heat transfer. The design of this ceramic HX is such that the area density is high and produces these corresponding results.

The base case results for the ceramic HX, by themselves, show encouraging heat transfer values, far greater than those of the 5-port, shell and tube bundle heat exchanger. A moderate level of enhancement, if able to eventually succeed, would be extremely favorable to any industry.

5.4 Summary

Results for the 5-port HX clearly show the possibilities of a commercially acceptable and manufacturable EHD heat exchanger. The maximum 2.7 fold enhancement achieved by the 5-port HX can be compared to a standard design tube-bundle HX nearly 3 times the size of the 5-port. A direct correlation cannot be exactly stated because the 3-fold increase is in heat transfer area, not any single dimension. The encouraging base case results for the ceramic HX, by themselves, show heat transfer values far greater than those of the 5-port metallic shell and tube bundle heat exchanger, on the order of three times that of the 5-port HX. As stated in section 2, heat exchangers with much greater β values can produce significantly higher heat transfer rates. This is clearly evident, albeit using a very different design, in comparing base case U values for each tested heat exchanger. If a method can be produced to incorporate the EHD technique for the ceramic heat exchanger, even a moderate level of enhancement would be significant, due to the fact that the base case heat transfer coefficients are already fairly high.

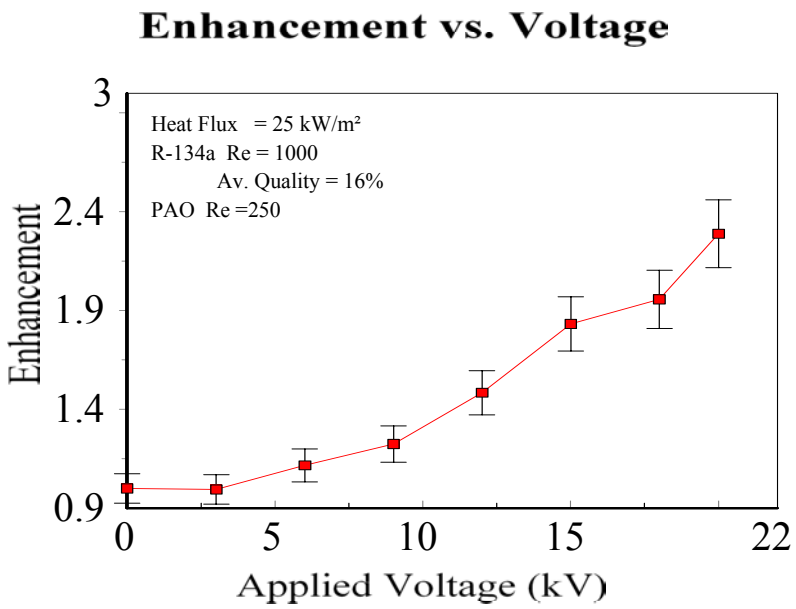

Figure 5.1 5-Port Metallic HX Enhancement Trand – Master Base Case

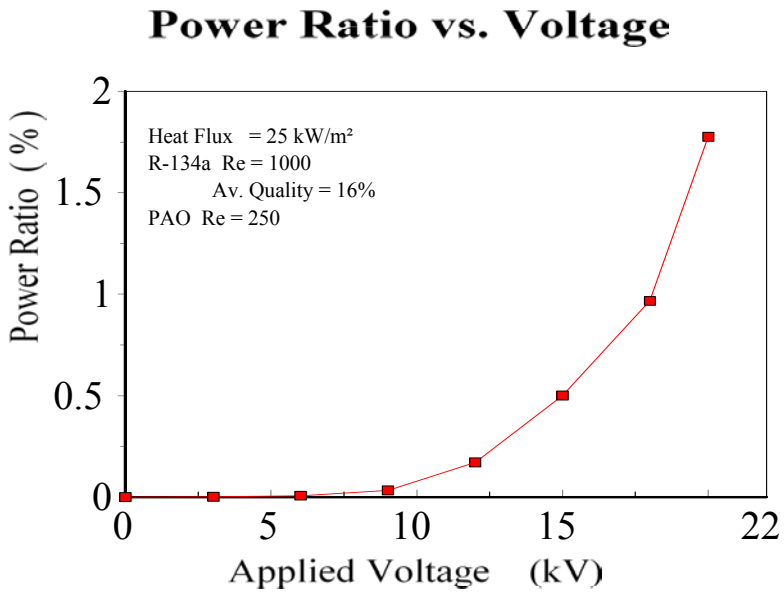

Figure 5.2 5-Port Metallic HX Power Ratio Trend – Master Base Case

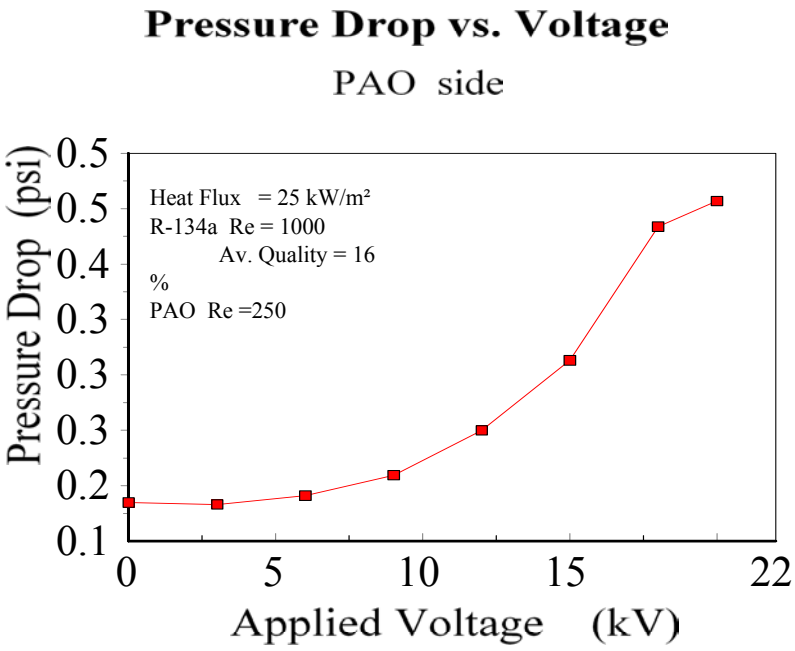

Figure 5.3 5-Port Metallic HX Pressure Drop Trend – Master Base Case

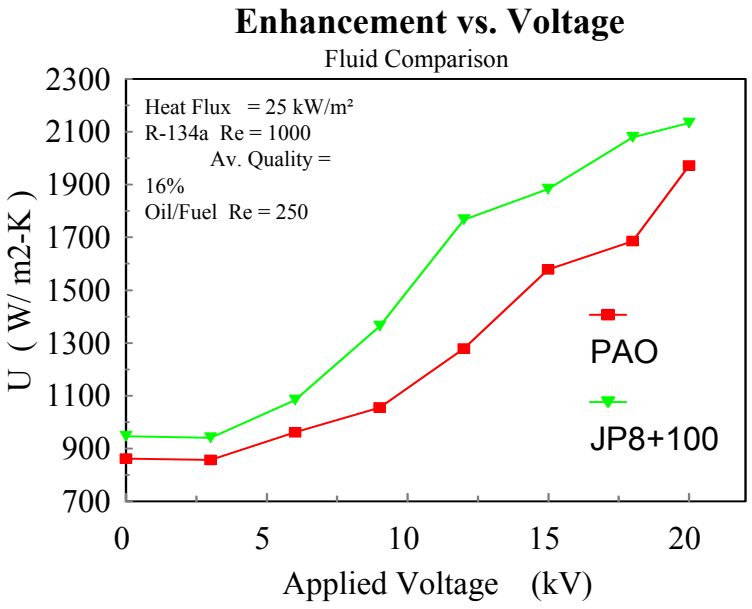

Figure 5.4 5-port Metallic HX Enhancement Comparison – Master Base Case

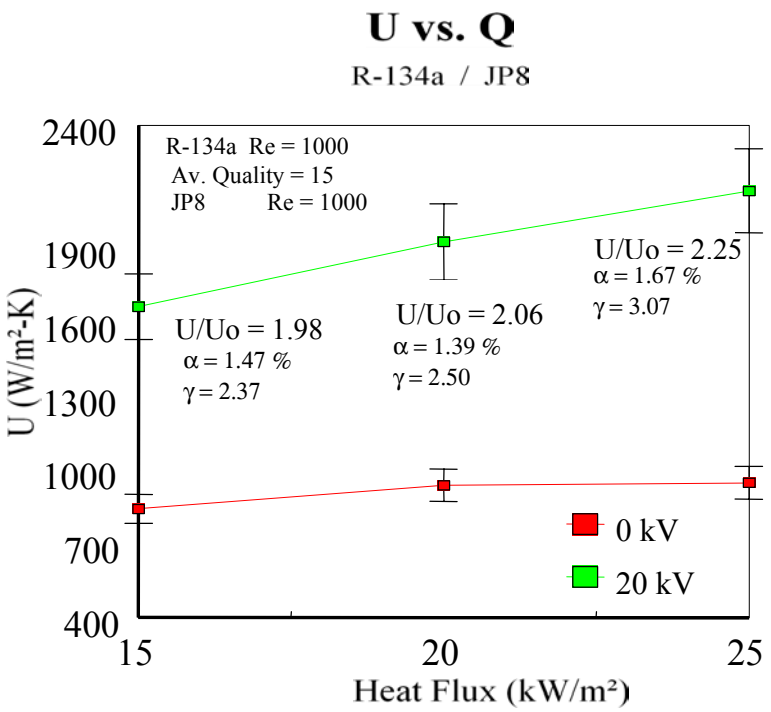

Figure 5.5 5-Port Metallic HX, U vs. Q for R-134a / JP8

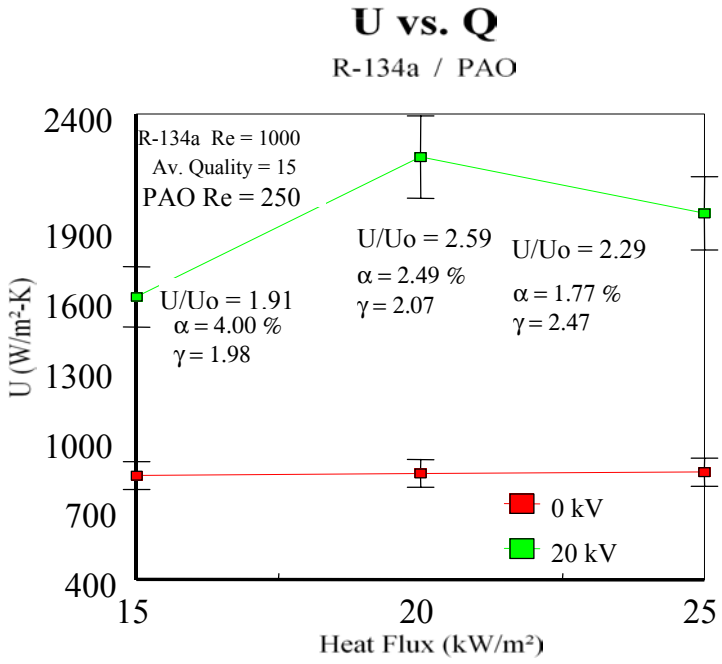

Figure 5.6 5-Port Metallic HX, U vs Q for R-134a / PAO

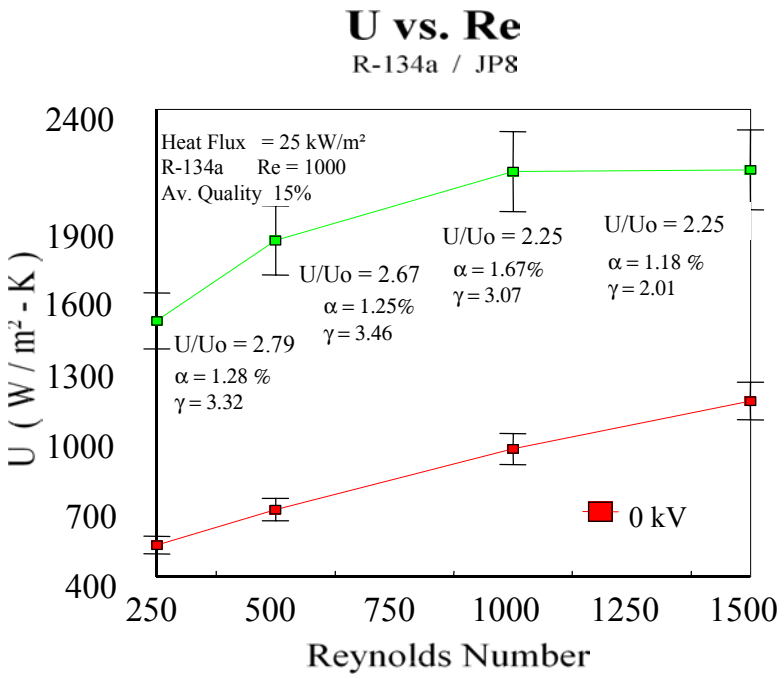

Figure 5.7 5-Port Metallic HX, U vs. Re for R-134a / JP8

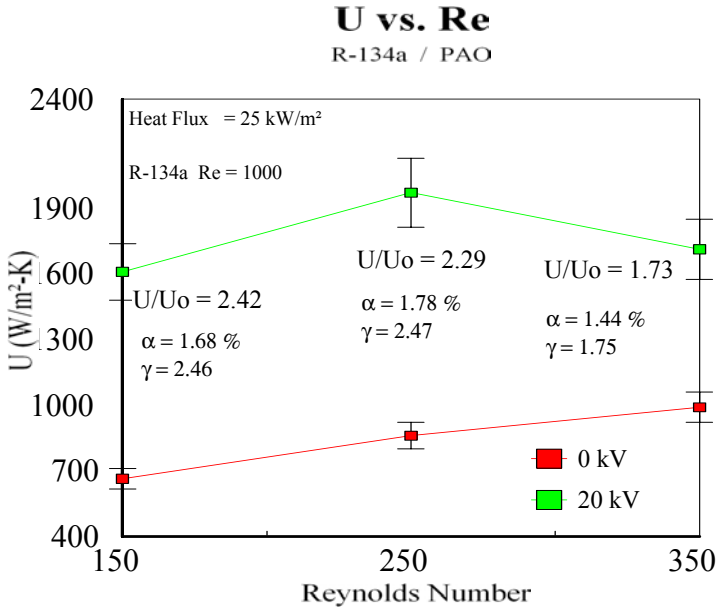

Figure 5.8 5-Port Metallic HX, U vs. R-134a / PAO

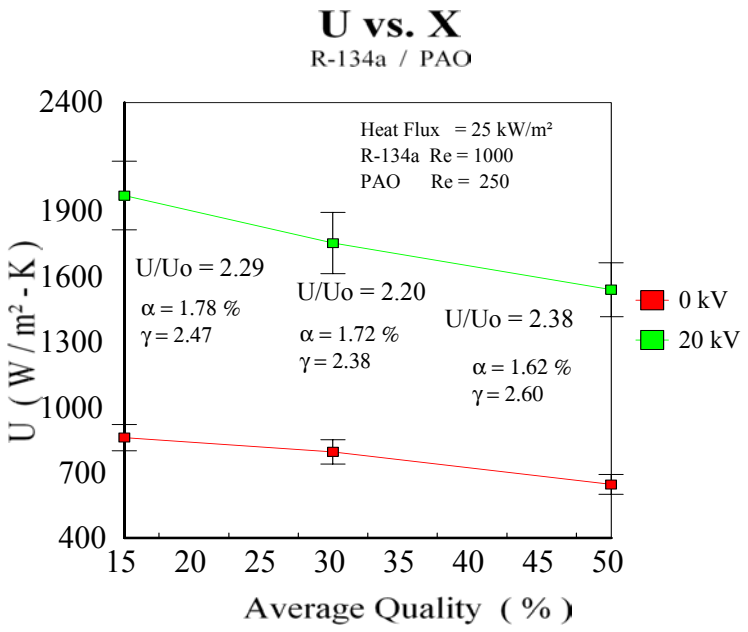

Figure 5.9 5-Port Metallic HX, U vs. X for R-134a / PAO

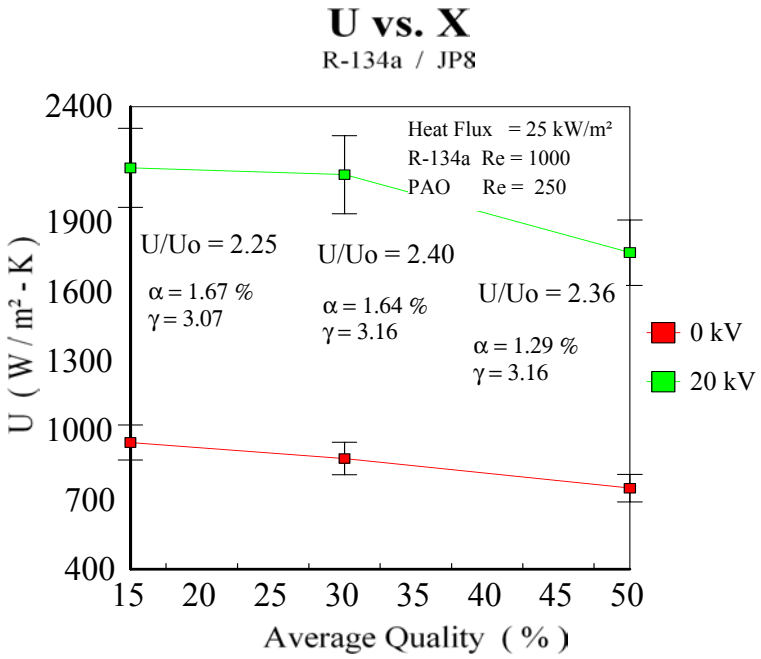

Figure 5.10 5-Port Metallic HX, U vs. X for R-134a / JP8

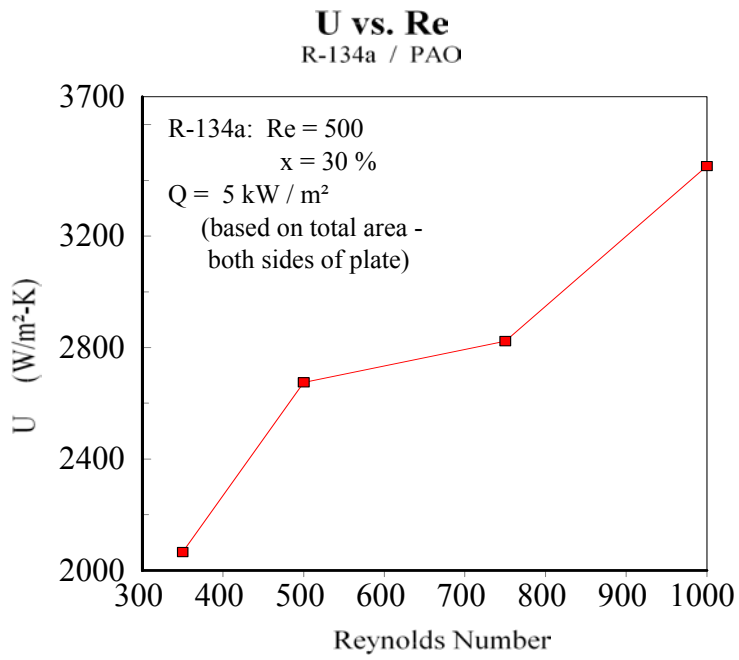

Figure 5.11 Ceramic HX U vs. PAO Re

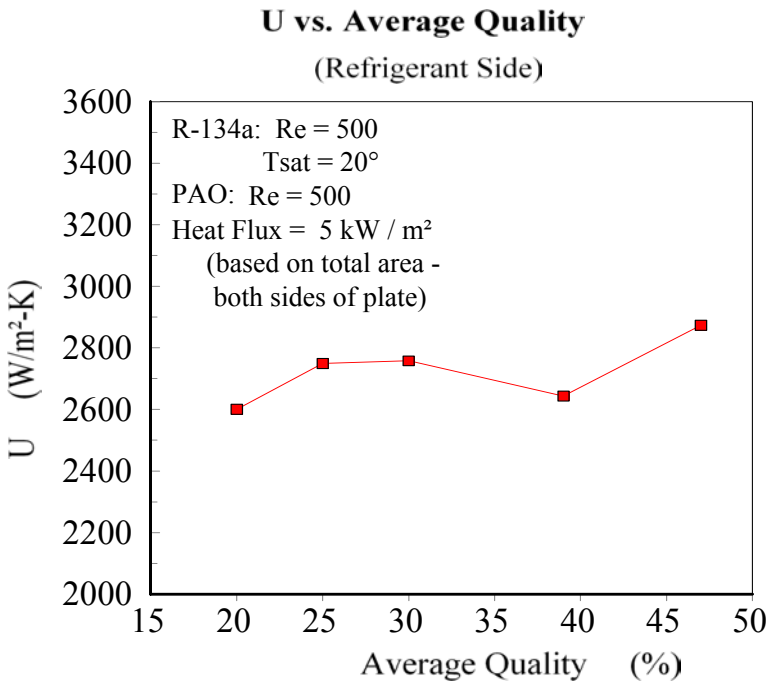

Figure 5.12 Ceramic HX U vs. Refrigerant Average Quality

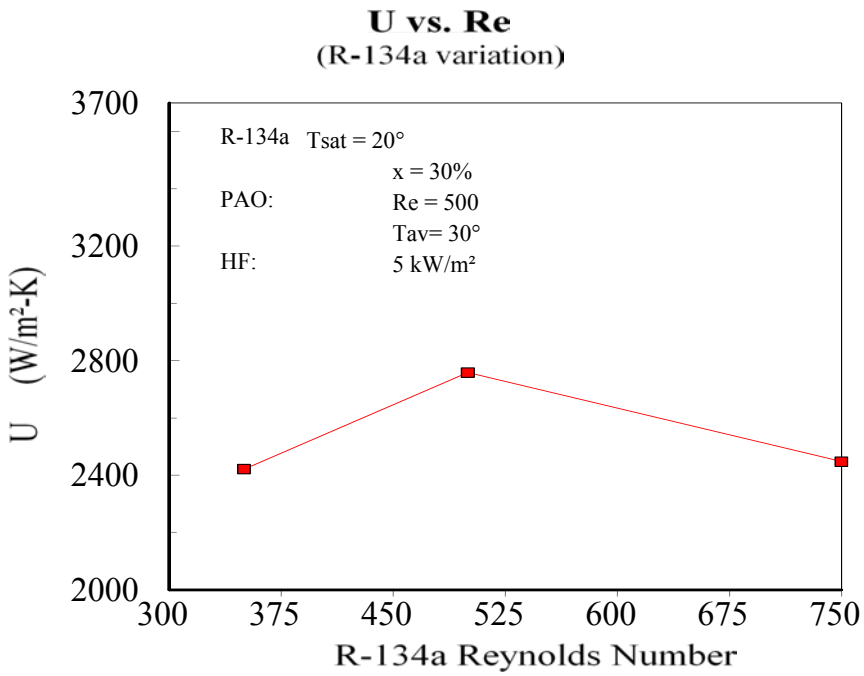

Figure 5.13 Ceramic HX U vs. Refrigerant Re

Chapter 6

DIFFICULTIES ENCOUNTERED, CONSIDERATIONS FOR FUTURE WORK, AND CONCLUSIONS

6.1 Introduction

As with most research experiments, many problems were encountered. Surprisingly, no problems of significance were attributed to the five-port metallic HX. Most of the problems occurred during testing of the ceramic heat exchanger. Numerous attempts to solve the problems were carried out, and are discussed here. Several iterations of design and test section modifications were completed, but with little success. There is legitimacy to the research, as this author has seen very favorable enhancement results premature to failure, but prior to steady state conditions and data recordation. Therefore, no evidence in the form of data exists due to the failures encountered. In the following sections, the main difficulties encountered are discussed, while research needs and future work are summarized. Finally, conclusions on the research will be presented.

6.2 Sealing Mechanism

The first design of the ceramic heat exchanger, unfortunately, fractured during installation before final pressure testing. The cause for this failure was the assumption that a standard O-ring would work for the gasket, when in fact, it did not. The O-ring was the correct size, in so far as circumference, but not configuration, and therefore, was difficult to keep perfectly in place during final closure and assembly of the test section frame. The O-ring gasket wanted to remain circular, thus causing the placement difficulty. The original test section design incorporated a 3 mm ledge around the entire

outer edge, in contrast to that shown in figure 4.5. When the O-ring was compressed for a good seal, the side with 9 channels had some failure. The edge of the outer fins tended to break off from the applied pressure.

The main fracture occurred when a very small portion of the O-ring was pinched under the corner of the test section. When the frame was assembled and tightened, the portion under the corner created a bending moment in the ceramic test section. Once enough force was applied around the entire frame, the ceramic snapped in half due to its brittle nature. An attempt was made to make our own gasket by cutting the correct size out of rubber sheeting material, but the results were not acceptable. Therefore, a mold was designed so that a rubber gasket could be poured and cured to exact specifications.

The second design iteration incorporated the self-manufactured, rectangular gasket made to fit around the test section and within the frame. To alleviate the problem of pressure fracturing the edge fins, a new, second ceramic plate design was manufactured with an extra 1 mm of material for the edge fins, so that the ledge had a dimension of only 2 mm in width, rather than 3 mm (figure 4.5). Once the manufactured gasket and new ceramic design were assembled, there were no fractures and the unit was properly sealed from cross-contamination.

6.3 Electrical Insulation

With the unit properly sealed and successfully pressure tested, the test section was inserted into the dual loop described in chapter 4. Experimentation commenced with base case scenarios shown in chapter 5. As the applied EHD field (voltage) was introduced into the test section, during the I-V characteristics curve test discussed in

chapter 4, problems were immediately apparent. This particular test was the one that the author witnessed enhancement. With very little applied voltage, 3 kV, well below typical onset voltage levels, temperatures were decreasing. Prior to equilibrium, the associated current values jumped significantly. This indicated an electrical short straight to ground. After considerable examination, it was determined that the rubber gasket was providing the conduit for the electrical flow. Once the electrical resistivity of the rubber was exceeded, the results were never duplicated. The manufactured gasket never regained the necessary electrical resistivity needed to maintain even low values of the required applied voltage across the fluid medium. The current followed the path of least resistance through the gasket and jumped the smaller gap between it and the high voltage plate, as depicted in figure 4.7. Two methods were considered to possibly resolve the issue. The first was a simple change in the size of the plate used to distribute the applied voltage. This change is shown as the final electrode configuration in figure 4.7. The change in distance was in the direction of fluid flow; however, increasing the distance did not resolve the problem. The distance perpendicular to channel length could not change; otherwise the outer channels would not be under the influence of high voltage. After consideration, it was determined that this was the path the short-to-ground traveled. The second considered method involved additional research into the actual gasket material. Styrene-Butadiene Rubber (SBR) was found to have an acceptable electrical resistivity, but after manufacture and testing, the SBR actually broke down under high voltages. Once this was realized, a 10^{16} ohm-cm resistivity alumina filled casting resin was used, but the final product was too rigid and brittle for use as the gasket. After additional, exhaustive research into a suitable gasket material, no solution was found in a timely

manner consistent with the sponsor's project schedule, resulting in abandonment of the ceramic HX research.

6.4 Conclusions

Electrohydrodynamic heat transfer, in this author's opinion, has been proven through this research that it is a viable and technologically sound method to improve heat transfer rates. Improved heat transfer rates will ultimately allow heat exchanger geometries to decrease to sizes more manageable for industries requiring electronic cooling, such as avionics, or other industries where reduced volumes are essential for success. The 5-port metallic, shell and tube heat exchanger described in this paper is already a unit of sufficient capacity to cool fluids using significantly less volume. Additionally, although the ceramic heat exchanger did not produce any enhancement data, the foundation for significant improvement has been laid.

The 5-port metallic, shell and tube heat exchanger, under EHD enhancement, was shown to increase the overall heat transfer coefficient up to 2.6 times using PAO in the enhanced shell side of the heat exchanger. JP8 was shown to increase up to 2.8 fold, also in the shell side. High heat fluxes and low Re flows are shown to be ideal for this technology to succeed. Power consumptions are minimal, especially when compared to high heat flux applications, where they have shown to be as low as 1.4%. The corresponding pressure drop increases, a detriment to any enhancement technology, are comparable to most methods, if not lower. Typically, the pressure drop increases were of the same magnitude as the increase in heat transfer. If additional research requirements such as transient response, power supply packaging, and internal tube enhancement,

produced significant success, this particular EHD heat exchanger would be very desirable in almost any commercial technology requiring the reduction of heat loads.

The ceramic heat exchanger, conversely, followed a research path in its infancy. Material research and investigation yielded significant knowledge into the properties of interest for heat transport development. Although there are currently only a handful of acceptable ceramics that could provide acceptable heat transfer, new ceramics are being developed and could be engineered to produce materials of desired properties. Detrimental properties such as brittleness, low elasticity, and low thermal conductivity could be engineered away in the future. For this research, the selection of Aluminum Nitride as the heat exchanger material incorporated the best available properties to allow insertion of the EHD technology. Unfortunately, the typical, inherent ceramic properties surfaced themselves and resulted in difficulties and setbacks.

While problems eventually halted the research due to sponsor time limits, encouraging non-EHD heat transfer results were achieved. The ability to achieve high overall heat transfer coefficients without enhancement, on the order of 3 times that of the 5-port metallic heat exchanger, but solely due to design, specifically using a high area density, gives hope to eventual success.

6.5 Future Work

The design, implementation, and experiments using the 5-port, shell and tube bundle heat exchanger encountered no significant problems, other than typical design optimizations and iterations to enhance expected performance. This heat exchanger is already a complete unit and, in the author's view, represents an excellent opportunity for

commercialization as a smart heat exchanger. Unlike conventional heat exchangers, the present HX unit can already provide on-line/on-demand capacity similar to those of standard configurations already on the market (see figure 4.2). Limits of allowable sizing for individual applications would need to be determined, as well as issues involving an appropriate power supply package consistent with the size of the heat exchanger and application scope. Two areas that could be investigated, however, would be development of a method allowing internal enhancement on the tube side, as well as transient response to sudden changes in heat load.

The main roadblock hindering success for the ceramic heat exchanger currently is the electrical insulation problem. Significant time must be spent in researching a suitable gasket material, or modified voltage connections so that the EHD technology can be demonstrated and successfully proven in a ceramic heat exchanger. Once proven, and enhancement values are documented, issues to be investigated are numerous. These include, but are not limited to, transfer of technology and materials to an actual heat exchanger unit, rather than a single plate heat exchanger, including the application of voltage to numerous HX plates. Other important aspects include durability, installation and/or mounting of the HX unit that would satisfy limiting factors discussed in chapter 3, i.e. brittleness, thermal shock, etc. as well as electrode testing. This testing should involve life cycle assessment and degradation of electrode material.

Reducing the EHD voltage required to produce enhancements would be a significant achievement. The witness of falling temperatures prior to failure of the ceramic HX test section well before the anticipated onset of enhancement could be the result of an unintended, smart electrode design. Considering the ground electrode was a

hand-painted silver finish, it could have provided sharp micro-inhomogeneities, greatly increasing the electrostrictive contribution well above expected values, thereby decreasing the level at which enhancement onset begins. Further research and development into this type of electrode design, coupled with high values of area densities, could lead to enhancement values considered unattainable even with today's enhancement technologies. Additionally, development is needed to produce cost effective components for the EHD system, most importantly, the high voltage power supply. This should be possible due to the very low current requirements (in the μA range) typically encountered with EHD studies, this one being no exception.

With any heat exchanger application involving EHD enhancement, long term effects of high electric field intensity upon the heat transfer fluids are, for the most part, unknown. Experiments involving continual and varying voltages should be required to verify whether or not the enhancements are repeatable over a period of time typical of most commercial systems. This could prove important as electrical resistivity of the heat transfer fluid medium may break down over time and not allow on-demand enhancement when required.

One of the goals of the current study using the ceramic test section was to incorporate two power supplies (as described in section 4.2), thereby enhancing both sides of the plate heat exchanger. This author believes that dual fluid enhancement incorporated into high area density heat exchangers using electrodes with micro-inhomogeneities will eventually be developed. This vision of successful future technology would be very desirable in the medical field considering bodily fluids are transported in channels of micron diameter proportions.

Many commercial applications of heat transfer involve the use of water, in both single and two-phase processes. Water is very abundant and has the most desirable heat transport properties. Unfortunately, water is not a fluid medium amenable to a high electric field. Future studies should look into the possibility of using de-ionized water, or the same, possibly seeded with types of particles that would allow application of a high voltage. There are more and more manufactured fluids interjected into the market every year. In the near future, there may be engineered fluids that possess water-like heat transport properties coupled with high enough electrical resistivities to sustain the necessary electric field intensities. Bodily fluids should be studied to determine what the effects of sustained voltage are, and if those effects would be harmful to humans, especially if technology were to advance to the level discussed in the previous paragraph concerning the medical profession.

Appendix A

Thermophysical Property Graphs

Density vs. Temperature for PAO

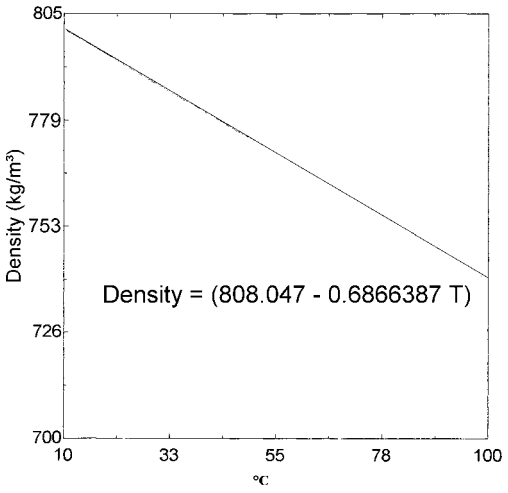

Kinematic Viscosity vs. Temperature for PAO

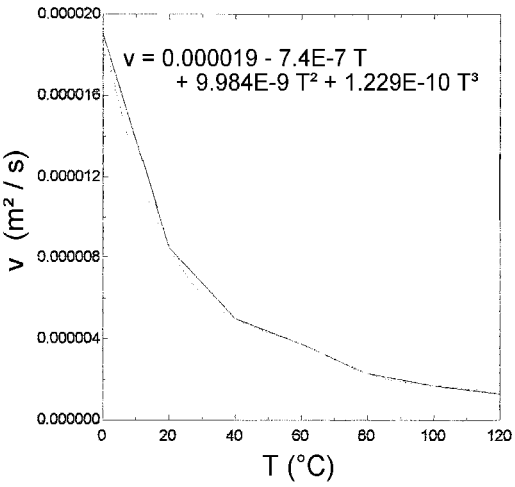

Specific Heat vs. Temperature for PAO

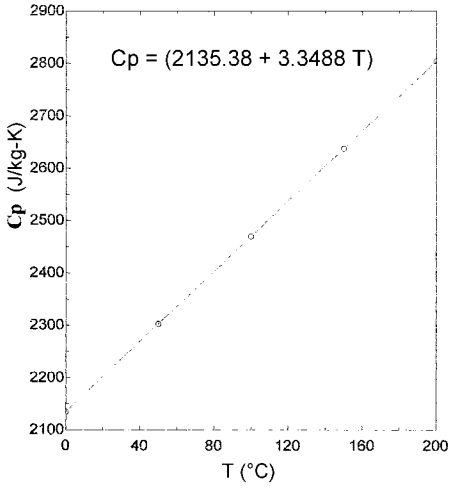

Thermal Conductivity vs. Temperature of PAO

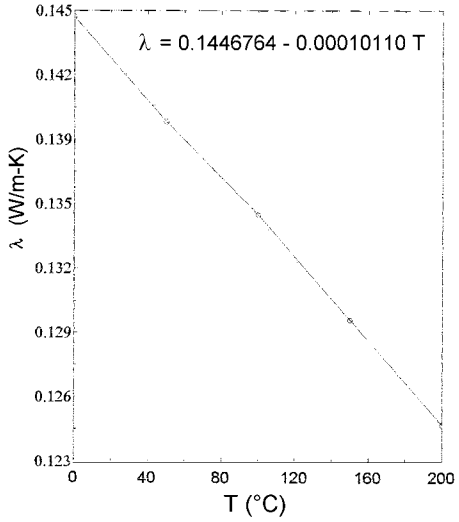

Density vs. Temperature for JP8

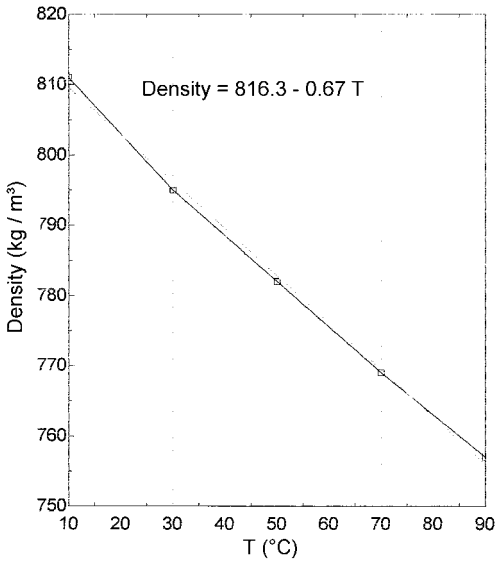

Kinematic Viscosity vs. Temperature for JP8

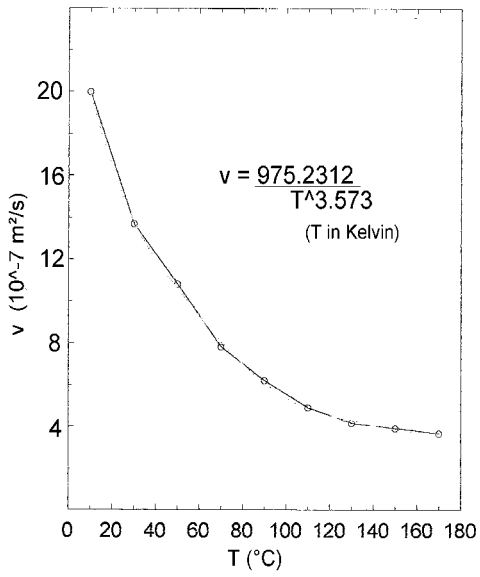

Specific Heat vs. Temperature for JP8

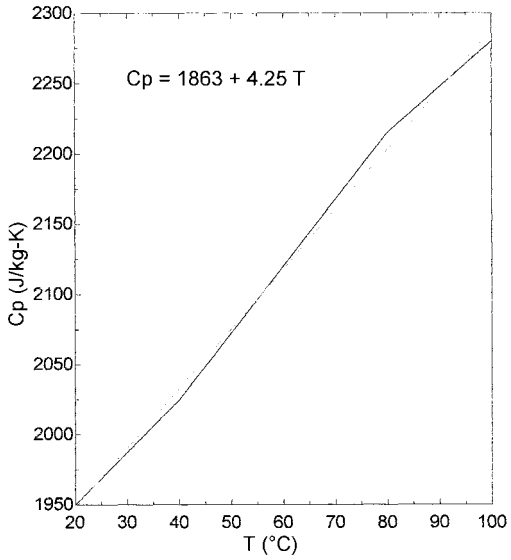

Thermal Conductivity vs. Temperature for JP8

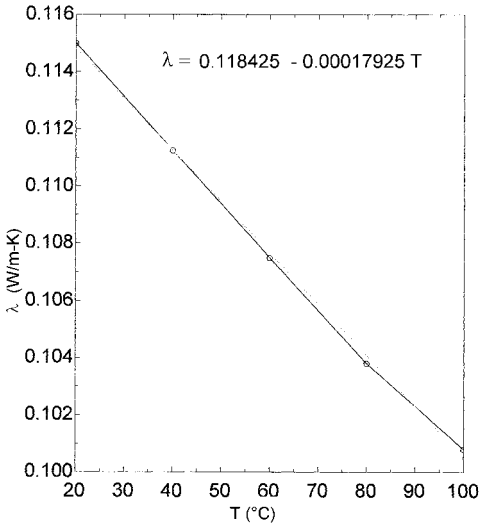

Appendix B

SAMPLE DATA SPREADSHEET

Heat transfer surface area = 0.0151613 m²

							Q needed to get x=0	68.19		
sub-cooled refgrig.	Ta	11.86								
	Tb	11.76	=>	T sub	11.82					
	Tc	11.84								
oil out	T1	46.34								
	T2	46.29	=>	Pao out	46.315					
						48.54				
oil in 2	T3	50.55								
	T4	50.53	=>	Pao in 2	50.54					
R134a out	T5	20.46					LMTD =	27.85		
	T6	20.3	=>	Ref out	20.38					
R134a in	T7	20.8					T sat =	20.62		
	T8	20.9	=>	Ref in	20.85	=>	h sat =	77.18		
oil in 1	T9	50.99					h fg =	180.5		
	T10	51	=>	Pao in 1	50.995					
oil	T11	46.07		Pao in	50.768					
bef. pump	T12	46.06	=>	Pao b pump	46.065		X in =	0		
	Ref DP V						h in =	77.19		
	Pao DP V	2.568	=>	DP =	0.1831	psi	X out =	0.32		
	Ref Htr V	70.4	=>	Q phtr =	68.267		h out =	135		
	Pao Htr V	99.2	=>	Q htr =	374.17		X avg =	0.16		
									Cp =	2.298
	Pao Pump V	8.6		+						
	Pao Pump I	1.3	=>	Q pump =	5.59					
	Ref Flow rate	323.64		=	----------		MF PAO =	33.52		
	appx. chiller T	18		Q in =	379.76					
	EHD Voltage	1.005	=>		3.015	kV	Q test sect. =	362.2		
	EHD Current	0.9	=>		0.0018	mA				
							U =	857.8		
				EHD Power	0.0054	Watts				
				Power Ratio	0.0014	%				

Appendix C

UNCERTAINTY ANALYSIS

A.1 Introduction

Experimental uncertainty analysis is the procedure used to quantify data validity and accuracy. The goal of this analysis was to estimate the uncertainty of experimental measurements and calculated results due to random errors. The procedure has two steps:

1. Estimate the uncertainty interval for each measured quantity.
2. Analyze the propagation of uncertainty into results calculated from experimental data.

A.2 Procedure

The uncertainties and standard deviations in a single measured independent variable x_1, x_2, … x_n are based on instrument accuracy and stated quantities from the manufacturer. Multiple measurements used to get an average will reduce the standard deviation in the following manner:

$$\sigma_{x\_avg} = \pm \frac{\sqrt{\sigma_{x1}{}^2 + \sigma_{x2}{}^2 + ... + \sigma_{xi}{}^2}}{i} \qquad \text{A.1}$$

Uncertainties are percentages that the deviation varies from the measured value, or:

$$u_Y = \frac{\sigma_Y}{Y} \qquad \text{A.2}$$

In many instances, measured values are required inputs into a formula to determine another desired value. In other words, the measurement of interest cannot be replicated directly. In these instances, a propagation of error formula must be used. The

propagation of error formula for: $Y = f(X, Z, ...)$ is:

$$u_Y = \sqrt{(u_x)^2 + (u_Z)^2 + ...} \qquad \text{A.3}$$

where $u_{x,z,...}$ are the uncertainties for each measured variable. To differentiate the difference between standard deviation and uncertainty, standard deviation values are ± values of identical units.

The experimental uncertainty associated with a sample test run for this research is presented next. First, a sample data values are presented in table A.1. (These measured/calculated values are taken from the sample data set shown in Appendix B.) Then each variable is discussed and its uncertainty is determined. Once each variable has a calculated uncertainty, the final quantity of interest's uncertainty, in this case, U, the Overall Heat Transfer Coefficient, can be calculated.

Table 1 Tabulated values with uncertainties

Variable	**Measured/Calculated Result**	**Uncertainty %**
C_P	2.30 kJ/kg-K	± 0.0005
ΔT	4.82 °C	± 0.21
Q_{pump}	5.59 W	± 4.32
Q_{htr}	374.17 W	± 6.00
Q_{PAO}	379.76 W	± 7.39
$\dot{m}$	32.70 g/sec	± 7.38
$Q_{test\ section}$	361.92 W	± 7.40
A	0.0151613 m²	± 1.89
LMTD	27.70	± 0.0186
U	861.77 W / m²-K	± 7.64

A.3 Determination of Standard Deviations and Uncertainties

The data reduction procedure, discussed in chapter 4, is more detailed. Here we will work in reverse to see which quantities are needed. Each of the final results during

experimentation, U is determined on the secondary loop by:

$$Q = U\ A\ LMTD \quad \Rightarrow \quad U = \frac{Q}{A\ LMTD} \tag{A.4}$$

Before continuation, standard deviations of Q, A, and LMTD are needed.

A.3.1 First Variable: Q The Q in this case is the total heat input into the test section. The formula used was:

$$Q = \dot{m}\, Cp\left(T_{in} - T_{out}\right) \tag{A.5}$$

C_P is temperature dependent and is evaluated at the entrance to the test section. The curve fit equation shown in appendix A (adjusted for unit consistency):

$$Cp = 2.135533 + (0.00335\ T) \tag{A.6}$$

The standard deviation associated with a temperature measurement is ±0.1 °C, but the inlet to the test section used two thermocouples, therefore, using equation A.1, the deviation in this temperature measurement, σ_T is ±0.071 °C. Using this value in equation A.2 and A.3, yields the uncertainty in Cp as u_{Cp} = ±0.0005 %, fairly insignificant.

The $\dot{m}$ in equation A.5 is the mass flux associated with the secondary fluid at the test section inlet. To determine $\dot{m}$, the inlet and outlet temperatures are determined from both sides of the heat input to the secondary flow by the pump and heater. The uncertainty in the temperature difference, $u_{\Delta T}$ is determined through the propagation equation, A.3, and yields $u_{\Delta T}$ = ±0.21 %. The uncertainty in the specific heat remains u_{Cp} = ±0.0005%. The Q input by the pump and heater are determined by Ohm's law relations using voltage, current, and resistance values. These formulas and associated

values input into equation A.3 yields $u_{Q\text{-}PAO} = \pm 7.43\%$. All uncertainties are calculated to now determine $u_{m\text{-}dot}$:

$$u_{\dot{m}} = \sqrt{\left(u_{Q_{PAO}}\right)^2 + \left(u_{C_P}\right)^2 + \left(u_{\Delta T}\right)^2} \qquad \text{A.7}$$

Substitution yields $u_{\dot{m}} = \pm 7.39\%$. Therefore, all values are now calculated and, after substitution, the uncertainty in $Q_{\text{Test Section}} = 7.4\%$.

A.3.2 Second Variable: A The area in this case is the heat transfer surface area of which the $Q_{\text{Test Section}}$ is applied, or:

$$A = N \pi D L \qquad \text{A.8}$$

where N is the number of tubes, D is the outside diameter of the tubes, and L is the effective length of the tubes. The uncertainty in A is more straightforward than the uncertainty in Q:

$$u_A = \sqrt{\left(u_D\right)^2 + \left(u_L\right)^2} \qquad \text{A.9}$$

N and π are numbers and do not affect the uncertainty in the area measurement. The standard deviation values for D and L are equal at $\sigma_x = \pm 0.00003$ m. After substitution, $u_A = 1.89\%$.

A.3.3 Third Variable: LMTD The logarithmic mean temperature difference is defined as:

$$LMTD = \frac{\left[\left(T_{h-in} - T_{c-out}\right) - \left(T_{h-out} - T_{c-in}\right)\right]}{\ln\left[\left(T_{h-in} - T_{c-out}\right) - \left(T_{h-out} - T_{c-in}\right)\right]} \qquad \text{A.10}$$

and the uncertainty:

$$u_{LMTD} = \{\left\{\frac{\left(T_{h-in} - T_{c-out}\right) - \left(T_{h-out} - T_{c-in}\right)}{\left(T_{h-in} - T_{c-out}\right)} - \ln\left[\frac{\left(T_{h-in} - T_{c-out}\right)}{\left(T_{h-out} - T_{c-in}\right)}\right]\right\}[u_{Th-out} + u_{Tc-out}]$$

$$+\left\{\frac{\left(T_{h-in} - T_{c-out}\right) - \left(T_{h-out} - T_{c-in}\right)}{\left(T_{h-out} - T_{c-in}\right)} - \ln\left[\frac{\left(T_{h-in} - T_{c-out}\right)}{\left(T_{h-out} - T_{c-in}\right)}\right]\right\}[u_{Th-in} + u_{Tc-in}]\} / \left\{\ln\left[\frac{\left(T_{h-in} - T_{c-out}\right)}{\left(T_{h-out} - T_{c-in}\right)}\right]\right\}^2$$

A.11

$u_{LMTD} = 0.0186\%$

A.4 Uncertainty in U Now that all values have been calculated u_U can be found by use of equation A.3 once again:

$$u_U = \sqrt{\left(u_Q\right)^2 + \left(u_A\right)^2 + \left(u_{LMTD}\right)^2} \qquad \text{A.12}$$

yielding:

$$u_U = 7.64\%.$$

REFERENCES

Barsoum, M., Fundamentals of Ceramics, McGraw Hill, New York, 1997

Bliem, C., Landini, D.J., Whitbeck, J.F., Kochan, R., Mittl, J.C., Piscitella, R., Schafer, J., Snyder, A., Wiggins, D.J., Zabriskie, J.M., Barna, B.A., Henslee, S.P., Kelsey, P.V., Federer, J.I., and Bomar, E.S., Ceramic Heat Exchanger Concepts and Materials Technology, Noyes Publications, Park Ridge, New Jersey, 1985

Choi, H.Y., "Electrohydrodynamic Condensation Heat Transfer," Transactions of the ASME, Journal of Heat Transfer, pp. 98-102, Feb. 1968

Colling, D.A., and Vasilos, T., Industrial Materials: Polymers, Ceramics, and Composites, Vol. 2. Prentice Hall, 1995

Custer, M., and Simpson, B., "Method of Making A Continuous Ceramic Fiber Reinforced Heat Exchanger Tube," U.S. Patent No. 5,575,067, Nov. 19, 1996

Haskin, W.L., and Paschkewitz, J.S., "Parameters for Aircraft EHD Heat Exchanger Development," SAE Aerospace Power Systems Conference, 98APSC-8, April 21-23, 1998

Heinrich, J., Huber, J., Schelter, H., Ganz, R., and Heinz, O., "Ceramic Heat Exchangers for Domestic and Industrial Application," Ceramics in Energy Applications: New Opportunities, Conference on Ceramics in Energy Applications, Session 4, April 1990

Holmes, R.E., and Chapman, A.J., "Condensation of Freon-114 in the Presence of a Strong Nonuniform, Alternating Electric Field," Transactions of the ASME, Journal of Heat Transfer, pp. 616-620, Nov. 1970

Landau, L.D., and Lifshitz, E.M., Electrodynamics of Continuous Media: Pergamon Press, pp. 64-69, 1960

Lashbrook, J., Holm, A., and Coston, K., "Ceramic Heat Exchanger Design," U.S. Patent No. 5,515,914, May 14, 1996

Linsner, O., Berroth, K., and Aktiengesellschaft, H., "Process for Sealing Ceramic Heat Exchangers," U.S. Patent No. 4,812,334, Mar. 14, 1989

London, A.L., "A Brief History of Compact Heat Exchanger Technology," ASME Winter Annual Meeting, HTD-Vol. 10, Nov. 16-21, 1980

Raj, P., "Aircraft Design in the 21st Century: Implications for Design Methods (Invited),"

29th AIAA Fluid Dynamics Conference, AIAA 98-2895, June 15-18, 1998

Stratton, J.A., Electromagnetic Theory, McGraw-Hill, New York, pp. 137-140,1941

Tran, T.N., Wambsganss, M.W., France, D.M., and Jendrzejczyk, J.A., "Boiling Heat Transfer in a Small, Horizontal, Rectangular Channel," AlChE Symposium Series, No. 295, Vol. 89, pp. 253-261, 1993

Woodson, H.H., and Melcher, J.R., Electromechanical Dynamics, Part II: Fields, Forces, and Motion," Robert E Krieger Publishing Company, pp. 463-465, 1985

Yabe, A, Taketani, T., Kikuchi, K., Yamashita, K., Kumagai, M., and Sekita, S., "Heat Transfer Characteristics on an EHD Condenser," ASME/JSME Thermal Engineering Proceedings, Vol. 3, pp. 61-67, 1991